

MAGNETOHYDRODYNAMICS

Magnetohydrodynamic (MHD) power generation is a method of generating electric power by passing an electrically conducting fluid through a magnetic field (see also Power generation). By means of the interaction of the conducting fluid with the magnetic field, the MHD generator transforms the internal energy of the conducting fluid into electric power in much the same way as a conventional turbogenerator does by means of the interaction of a solid conductor with a magnetic field. In principle, the working fluid can be any electrically conducting fluid, such as salt water, liquid metal, or hot ionized gas. For central station power generation applications, the most suitable working fluid is a hot ionized gas. This can be a relatively clean gas, eg, a noble gas (see Helium group, gases) heated in an externally fired heat exchanger, or it can be composed of combustion products from any fossil fuel. There are two basic types of MHD energy conversion systems. Closed cycle typically operates using a clean gas which is recycled; open cycle generally operates using combustion products which are then discarded.

In its simplest form the MHD generator consists of a duct through which the gas flows, driven by an applied pressure gradient, and a magnet, in which the duct is located. The generator operates in a Brayton cycle similar to that of a turbine. Because the MHD process requires no rotating machinery or moving mechanical parts, the MHD generator can operate at much higher temperature and hence, higher efficiency, than is possible for other power generation technologies. The system of most interest for central station power generation is the open cycle system using electrically conducting coal (qv) combustion products as the working fluid. Coal-burning central station MHD power plants promise to generate power at up to 50% greater efficiency and at a lower cost of electricity than can be achieved using conventional coal-burning power plants of the early to mid-1990s (see Coal conversion processes).

In addition to potential advantages in efficiency, MHD power generation offers significant potential for reduced environmental intrusion. Effective control of pollutants is inherent in the basic design and operation of MHD power plants. Emissions of SO_x , NO_x , and particulates can be reduced to levels far below the New Source Performance Standards (NSPS) of 1979 without requiring expensive gas clean-up equipment. Furthermore, because of the higher efficiency and consequent lower fuel usage of MHD power plants, emissions of carbon dioxide (qv) are lower, heat rejection is reduced, and less solid waste is produced (see Air pollution; Wastes, industrial). The basic principle of MHD power generation was discovered in 1831 by Michael Faraday (1), who investigated electromagnetic interactions induced by the flow of the Thames River in the magnetic field of the earth. The first serious attempts at MHD power generation were made between 1936 and 1945 (2). The first successful MHD generator was built in 1959 (3–5). This device operated on argon heated to high temperatures by a plasma jet, and produced 11.5 kilowatts of power. A combustion-driven generator of approximately the same size was built in 1960 (6), and achieved continuous operation for about one hour. A much larger combustion-driven generator which produced about 1.5 megawatts of electrical power was built by Avco in 1962 (7). Measured performance was in close agreement with theoretically predicted results.

2 MAGNETOHYDRODYNAMICS

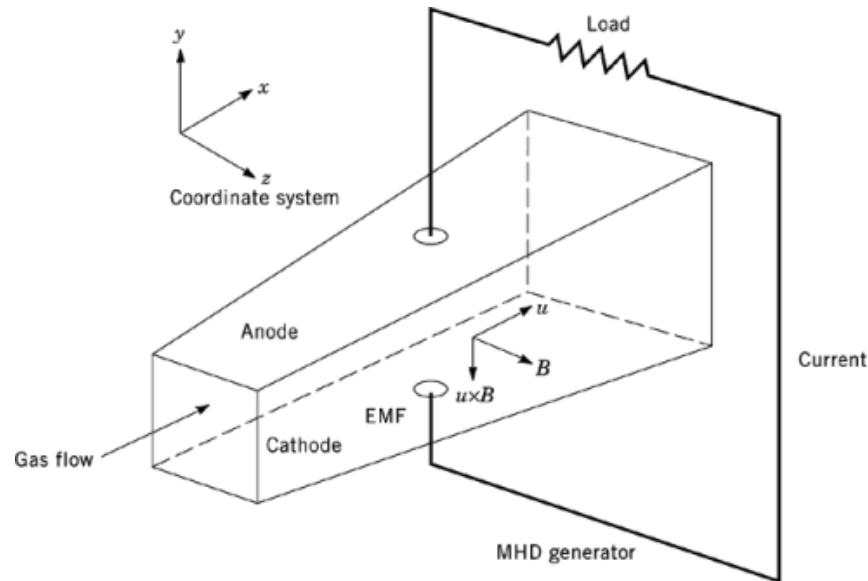


Fig. 1. Principles of MHD. See text.

1. System Components

The implementation of the Faraday effect to produce MHD power is shown in Figure 1. An electrically conducting fluid flows with velocity \vec{u} , through a magnetic field \vec{B} , to induce an electric field \vec{E} which is orthogonal to both the flow direction and the magnetic field direction. If the flow is contained in a duct, as shown, the two walls perpendicular to the electric field are at different potentials. If these two walls are electrically conducting and connected through an external resistance or load, the field causes a current to flow through the load, thus generating power. The conducting walls, through which current is extracted from the duct, are the electrode walls. The wall which emits electrons is designated the cathode; the other wall is the anode. The two walls separating the electrode walls are the insulator walls.

For central station power generation the open cycle system using electrically conducting coal combustion products as the working fluid is employed. The fuel typically is pulverized coal burned directly in the MHD combustor, although in some plant designs cleaner fuels made from coal by gasification or by beneficiation have been considered (8–10) (see Fuels, synthetic).

In application to electric utility power generation, MHD is combined with steam (qv) power generation, as shown in Figure 2. The MHD generator is used as a topping unit to the steam bottoming plant. From a thermodynamic point of view, the system is a combined cycle. The MHD generator operates in a Brayton cycle, similar to a gas turbine; the steam plant operates in a conventional Rankine cycle (11).

Starting with combustion products at a pressure of 0.5–1 MPa (5–10 atm), and a temperature sufficiently high (ca 3000 K) to produce a working fluid of adequate electric conductivity when seeded with an easily ionizable salt such as potassium carbonate or formate, the hot ionized gases flow through the MHD generator at approximately sonic velocity. The MHD generator duct, or channel, extracts energy from the gas, and the flow is expanded so that it can maintain its velocity against the decelerating forces resulting from its interaction with the magnetic field. The combination of energy extraction and flow expansion causes the gas temperature to drop. Energy is extracted until the gas temperature becomes too low (ca 2300 K) to have a useful electric conductivity.

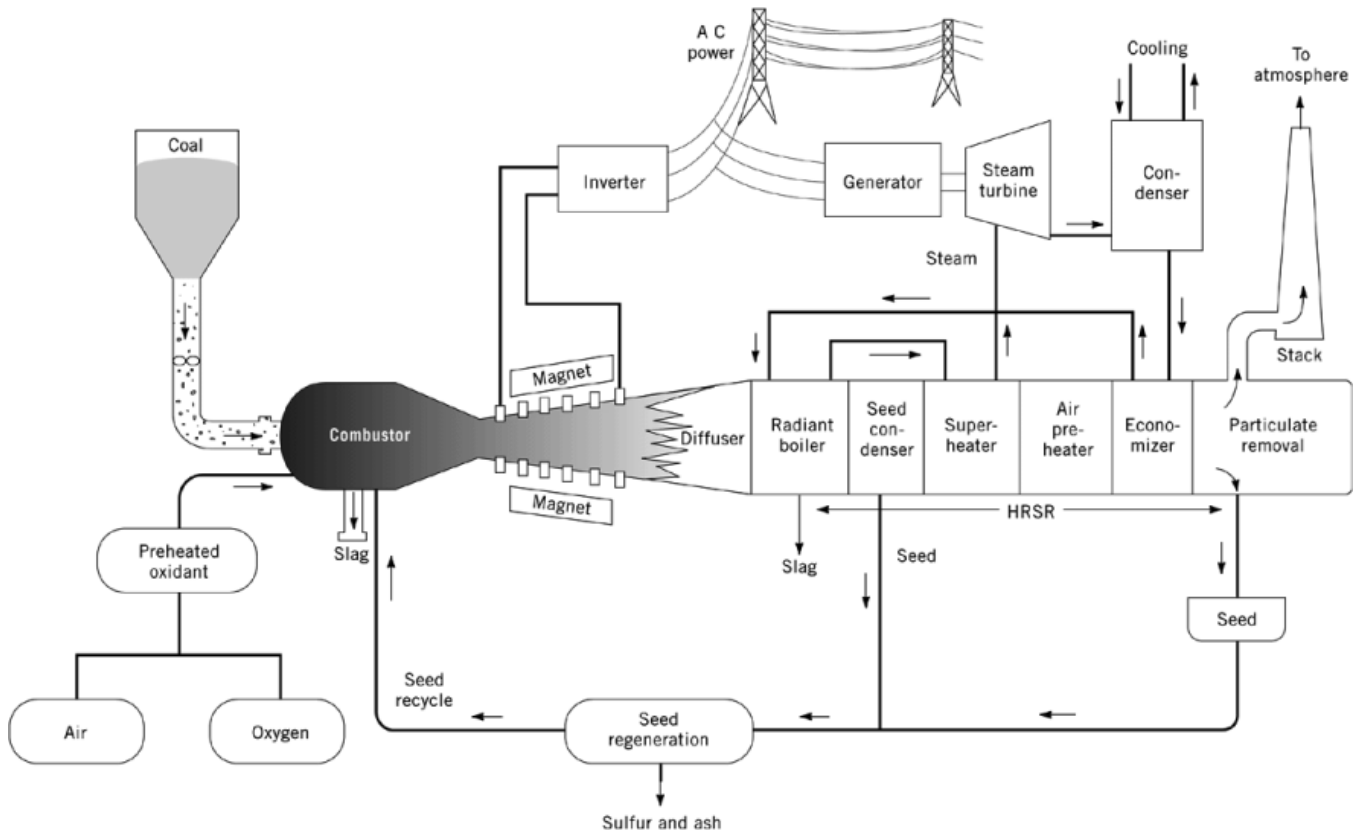


Fig. 2. MHD-steam power plant where HRSR is heat recovery seed recovery and the seed is an easily ionizable potassium salt. See text.

The gases exhausting from the generator still contain significant useful heat energy. This energy is used in the bottoming plant to raise steam to drive a turbine and generate additional electricity in the conventional manner of a steam plant. The generator exhaust gases also contain potassium and sulfur from the coal. These combine to form primarily potassium sulfate, which condenses in the bottoming plant and is then delivered to a seed regeneration unit where it is converted back to potassium formate or carbonate and recycled to the MHD combustor.

The required high combustion temperatures can be achieved by preheating the combustion air to temperatures of 1650–1950 K. The highest efficiencies are obtained by direct high temperature preheat of the combustion air with the MHD exhaust gas, but this requires the use of high temperature refractory heat exchangers, which are not commercially available. The requisite combustion temperatures can also be attained by enriching the combustion air with oxygen and preheating the oxygen-enriched air to more moderate temperatures, which can be reached in conventional metal tubular heat exchangers. The resultant plant efficiencies are high enough to make this latter method attractive for use in first generation commercial plants based on available technology. High temperature refractory heat exchangers would allow realization of the full efficiency potential of MHD as well as improved fuel utilization, and even lower energy costs (see Refractories).

Other MHD power cycles have been proposed in which the heat energy of the MHD generator exhaust gas is utilized in a bottoming gas turbine plant (12, 13). The gas turbine working fluid in such a plant is clean air heated by the MHD generator exhaust gas. Efficiency advantages offered by the use of a high temperature

4 MAGNETOHYDRODYNAMICS

gas (air) turbine instead of a steam turbine in the bottoming plant should improve the overall MHD power cycle accordingly. MHD power cycles of this type do not need cooling water for steam condensation and heat rejection.

The components of a combined MHD–steam power plant which are most directly associated with the MHD process are referred to collectively as the MHD power train, or as the topping cycle components. The rest of the plant consists of the steam bottoming plant, a cycle compressor, the seed regeneration plant, and the oxygen plant, if necessary. The MHD topping cycle components are the magnet, the coal combustor, nozzle, MHD channel, associated power conditioning equipment, and the diffuser. The magnetic field required in a commercial plant is typically 4.5–6 tesla ($4.5 - 6 \times 10^4$ G). Hence, the magnet is superconducting, as a conventional magnet would require impractical amounts of electric power (see Magnetic materials).

Power conditioning is necessary between the channel and the transmission grids for two reasons. First, the channel produces d-c electric power, because both the magnetic field and the channel flow are nominally time-invariant. Therefore, an inverter is required to convert the d-c MHD output to a-c for transmission. Voltage step-up is also required, as the generator output is typically at lower voltage (20–40 kV) than that required for transmission. Second, a large channel may have a large number of two terminal outputs, and circuitry is needed to consolidate the outputs from all the terminal pairs for delivery into the main load inverter.

The steam bottoming plant of the combined MHD–steam power plant consists basically of a heat recovery and seed recovery system (HRSR) and a turbine–generator for additional power production. The HRSR is essentially a heat recovery boiler and oxidant preheater which is fired by the exhaust gases from the MHD channel. In addition to generating steam, the HRSR system must also perform the functions of NO_x and SO_x control, slag tapping, seed recovery, and particulate removal (see Air pollution control methods; Exhaust control, industrial).

1.1. Chemical Regeneration

In most MHD system designs the gas exiting the topping cycle exhausts either into a radiant boiler and is used to raise steam, or it exhausts into a direct-fired air heater and is used to preheat the primary combustion air. An alternative use of the exhaust gas is for chemical regeneration, in which the exhaust gases are used to process the fuel from its as-received form into a more beneficial one. Chemical regeneration has been proposed for use with natural gas and oil as well as with coal (14) (see Gas, natural; Petroleum).

A coal-based system (Fig. 3) is described in References 15 and 16. The generator exhaust gas is used in a multistage process in which the incoming coal undergoes devolatilization, gasification, and partial combustion at atmospheric pressure to produce a low heating value (LHV) fuel gas for the primary combustor. The thermal energy recovered from the exhaust gas and stored in the fuel gas is roughly 40% of the combustion energy of the fuel into the primary combustor (15), so that a substantial increase in fuel energy is achieved by use of chemical regeneration. An alternative scheme would be to locate the regenerator upstream of the MHD generator so that gasification is done at peak cycle pressure. The advantage of this system is that a smaller volume of gas is processed. Variations of this scheme are described elsewhere (17–19). Comparisons of cycles which use the generator exhaust gas to preheat combustion air to cycles which use chemical regeneration can be found in Reference 15. Somewhat higher efficiencies can be obtained with the use of chemical regeneration than without, for a given cycle pressure ratio.

2. MHD Fundamentals

The basic principles of MHD power generation are shown in Figure 1. The working fluid is typically a slightly ionized gas, ie, mostly neutral atoms or molecules where a small ($<0.1\%$) fraction are ions and electrons. The working fluid flows with velocity u , in the axial, x , direction, through the MHD channel, which is located in a

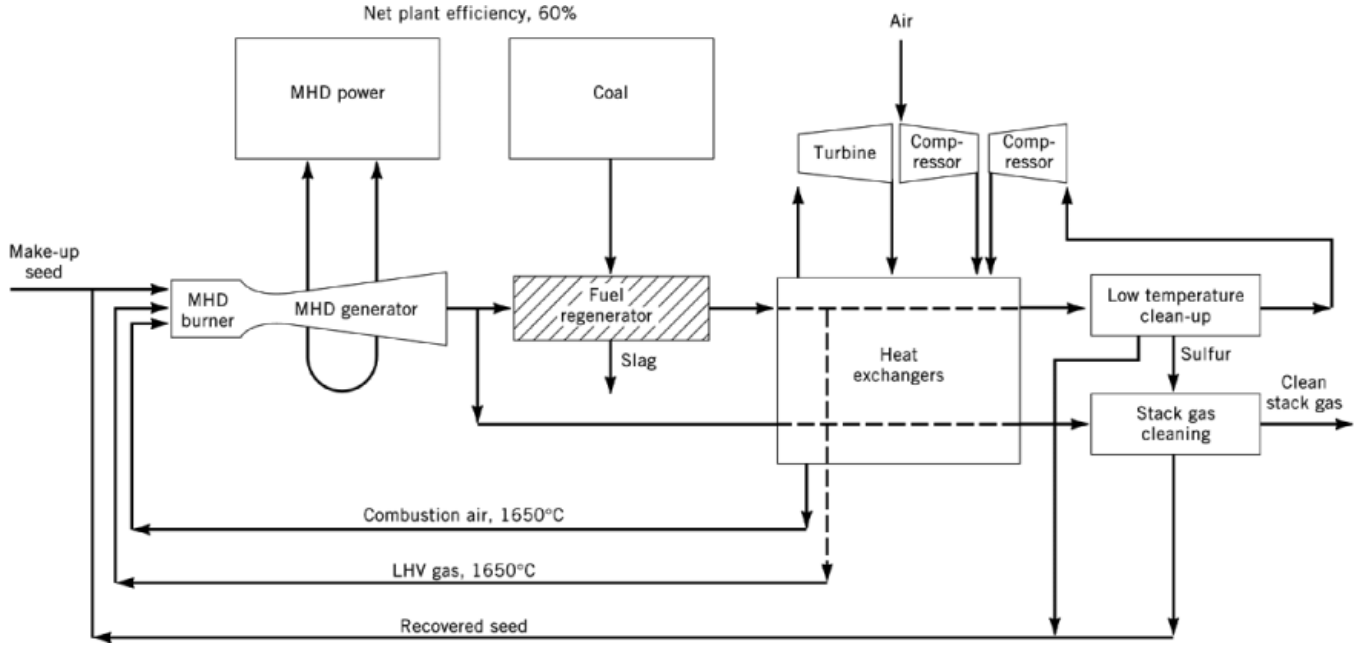


Fig. 3. MHD power plant design burning low heating value (LHV) gas produced from coal by chemical regeneration.

magnetic field of strength B , in the z direction. An electric field, uB , is induced in the transverse ($-y$) direction, as shown. Because there exists also an internal electric field, E' , owing to the load current, the electric field, E' , seen by the moving gas is

$$E' = E - uB \quad (1)$$

and the induced current per unit area, j_y , is

$$j_y = \sigma E' = \sigma (E - uB) \quad (2)$$

where σ is the electrical conductivity of the gas. If a load coefficient K is defined, such that

$$K \equiv E/uB \quad (3)$$

the magnitude, j , of the current density can be expressed as

$$j = \sigma uB(1 - K) \quad (4)$$

and the generator power per unit volume, P , is then

$$P = jE = \sigma u^2 B^2 K(1 - K) \quad (5)$$

Assuming that the current in the gas is carried mostly by electrons, the induced electric field uB causes transverse electron motion (electron drift), which, being itself orthogonal to the magnetic field, induces an

6 MAGNETOHYDRODYNAMICS

axial electric field, known as the Hall field, and an axial body force, F , given by

$$F = jB = \sigma u B^2 (1 - K) \quad (6)$$

This force acts in the $-x$ direction and retards the flow. The rate at which the gas does work in pushing itself against this force is

$$Fu = jBu = \sigma u^2 B^2 (1 - K) \quad (7)$$

The ratio of electrical power output (eq. 5) to the power required to push the gas (eq. 7) can be defined as the efficiency of the process, η_e :

$$\eta_e = jE/juB = K \quad (8)$$

The difference between the push power and the electric power output is

$$juB - jE = j^2/\sigma \quad (9)$$

The term j^2/σ is the rate of dissipation of energy per unit volume by joule heating. This occurs within the working fluid, and so represents a departure from thermodynamic irreversibility rather than an energy loss.

This simplified discussion has neglected the effects of axial current flow, ie, Hall current, induced by the axial field. At a local region in the channel, equation 1 can be written in more general form as

$$\vec{E}' = \vec{E} + \vec{u} \times \vec{B} \quad (10)$$

The electrons move with a drift velocity \vec{v}_e relative to the gas. Then the electric field \vec{E}' felt by the electrons is

$$\vec{E}' = \vec{E} + \vec{u} \times \vec{B} + \vec{v}_e \times \vec{B} \quad (11)$$

The electron current density \vec{j}_e is

$$\vec{j}_e = \sigma \vec{E}' = \sigma (\vec{E} + \vec{u} \times \vec{B} + \vec{v}_e \times \vec{B}) \quad (12)$$

Electron current density can also be expressed as

$$\vec{j}_e = -n_e \vec{v}_e e \quad (13)$$

where n_e is the electron number density and e the electron charge. The equation has a minus sign because the electron charge is negative and current flow is conventionally defined as the flux of positive charges.

The electrical conductivity σ can be expressed in terms of the mobility μ_e :

$$\sigma = n_e \mu_e e \quad (14)$$

Using equations 13 and 14 in equation 12, the current density can be expressed as

$$\vec{j}_e = \sigma (\vec{E} + \vec{u} \times \vec{B}) - \mu_e (\vec{j}_e \times \vec{B}) \quad (15)$$

The first term on the right represents scalar conduction and the second term the Hall effect. This is generally expressed in terms of the Hall parameter $\beta = \mu_e B$, so that

$$\vec{j}_e = \sigma (\vec{E} + \vec{u} \times \vec{B}) - \frac{\beta}{B} (\vec{j}_e \times \vec{B}) \quad (16)$$

Equation 16 is a form of the generalized Ohm's law. Ion mobility, electron pressure gradients, and inertial effects have been neglected. The latter two phenomena are generally of no concern in MHD generator flows, but ion mobility is sometimes significant. Ohm's law including ion mobility, stated here without proof, is

$$\vec{j} = \sigma (\vec{E} + \vec{u} \times \vec{B}) - \frac{\beta}{B} (\vec{j} \times \vec{B}) + \frac{\beta\beta_i}{B^2} (\vec{j} \times \vec{B}) \times \vec{B} \quad (17)$$

where β_i , the Hall parameter, $= \mu_i B$; μ_i is the ion mobility. A derivation of equation 17 which is valid for weakly ionized gases, ie, the fraction of ionized atoms is small, can be found in Reference 20.

Equation 17 can be solved for the components of \vec{j} . In the coordinate system of Figure 1, with \vec{B} in the z direction and \vec{u} in the x direction, $u_x = u$, $u_y = u_z = 0$; $B_z = B$, $B_x = B_y = 0$; $E_z = 0$. Then,

$$j_x = \frac{\sigma}{(1 + \beta\beta_i)} E_x - \frac{\beta}{(1 + \beta\beta_i)} j_y \quad (18)$$

$$j_y = \frac{\sigma}{(1 + \beta\beta_i)} (E_y - uB) + \frac{\beta}{(1 + \beta\beta_i)} j_x \quad (19)$$

$$j_z = 0 \quad (20)$$

The ratio β_i/β is the ratio of ion mobility to electron mobility, μ_i/μ_e , which is approximately the square root of the ratio of electron mass to ion mass. For potassium seed material in combustion gases, μ_i/μ_e is about 0.003. Therefore $\beta_i/\beta \approx 0.003$, and, for typical values of β , $1 \lesssim \beta \lesssim 3$, $(1 + \beta\beta_i) \approx 1$. Equations 18 and 19 then reduce to the following:

$$j_x = \sigma E_x - \beta j_y \quad (21)$$

$$j_y = \sigma (E_y - uB) + \beta j_x \quad (22)$$

As shown in equation 6, an axial force jB , or, more generally, $\vec{j} \times \vec{B}$, is induced by the transverse current flow. Most of the current is carried by the electrons owing to their much greater mobility compared to the ions. The axial force is therefore felt primarily by the electrons, but is communicated to the ions via Coulomb interactions. As a result, the electrons and ions together begin to move with a slip velocity relative to the neutral particles in the flow, and a steady state is reached in which the slip momentum is transferred to the neutrals via collisions. This is the process by which the $\vec{j} \times \vec{B}$ force is transferred from the current carriers to the gas as a whole and

8 MAGNETOHYDRODYNAMICS

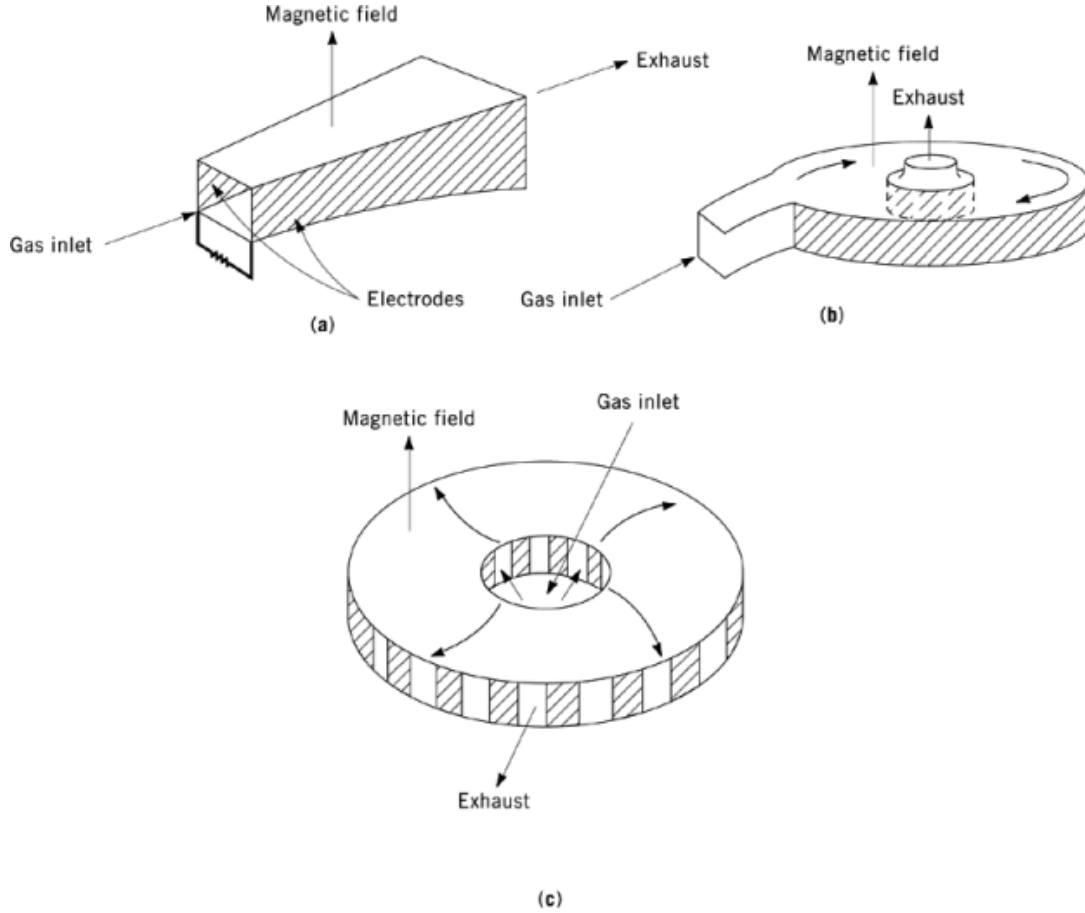


Fig. 4. MHD generator geometries: (a), linear; (b), vortex; and (c), disk having radial outflow.

is the mechanism through which the kinetic and thermal energy of the gas is converted to the electrical energy extracted from the flow. The $\vec{j} \times \vec{B}$ force is known as the Lorentz force and acts to oppose the gas flow.

2.1. MHD Generator Geometries

The basic requirement for any generator geometry is that the gas velocity have a component that is not parallel to the magnetic field. For efficiency, the gas velocity should be orthogonal to the magnetic field direction. Some of the possible geometries for achieving this are shown in Figure 4. Development work has focused mainly on the linear generator (Fig. 4a). Detailed descriptions of the disk and vortex configurations can be found in References 21 and 22, respectively.

There are four basic variations of the linear MHD channel (Fig. 5) which differ primarily in their method of electrical loading. The simplest is the two-terminal Faraday or continuous electrode generator, Figure 5a, where a single pair of current-collecting electrodes spans the channel in the axial direction, short-circuiting the channel from end to end. Hence, for this configuration, $E_x = 0$, and j_y can be obtained from equations 21

and 22:

$$j_y = \frac{\sigma}{1 + \beta^2} (E_y - uB) \quad (23)$$

Additionally, there exists an axial or Hall current j_x given by

$$j_x = -\frac{\sigma\beta}{1 + \beta^2} (E_y - uB) \quad (24)$$

The generator power output per unit volume P is

$$P = -\vec{E} \cdot \vec{j} = -E_y j_y = -\frac{1}{1 + \beta^2} \sigma (E_y - uB) E_y \quad (25)$$

In terms of the load parameter, $K = E/uB$,

$$P = \frac{\sigma u^2 B^2}{1 + \beta^2} K(1 - K) \quad (26)$$

Compared to the expression of equation 5, having no axial current flow, power output is reduced by the factor $1/(1 + \beta^2)$. This is because part of the kinetic and thermal energy of the gas generates the axial current j_x which flows upstream in the gas and returns through the electrode walls. This current does not flow through the external load and so represents a loss./clearpage

The axial current flow can be eliminated, and so the power output increased, by axial segmentation of the electrodes, as shown in Figure 5b, the segmented Faraday generator. Each opposing pair of electrodes is connected to a single load. The axial electrode segments are separated by insulators, thus preventing axial current flow, ie, $j_x = 0$. Then the transverse current j_y becomes

$$j_y = \sigma (E_y - uB) \quad (27)$$

The power density is

$$P = \sigma u^2 B^2 K(1 - K) \quad (28)$$

and an axial field, E_x , is developed, given by

$$E_x = \beta (E_y - uB) \quad (29)$$

In practice, elimination of axial current flow requires relatively fine segmentation, eg, 1–2 cm, between electrodes, which means that a utility-sized generator contains several hundred electrode pairs. Thus, one of the costs paid for the increased performance is the larger number of components and increased mechanical complexity compared to the two-terminal Faraday generator. Another cost is incurred by the increased complexity

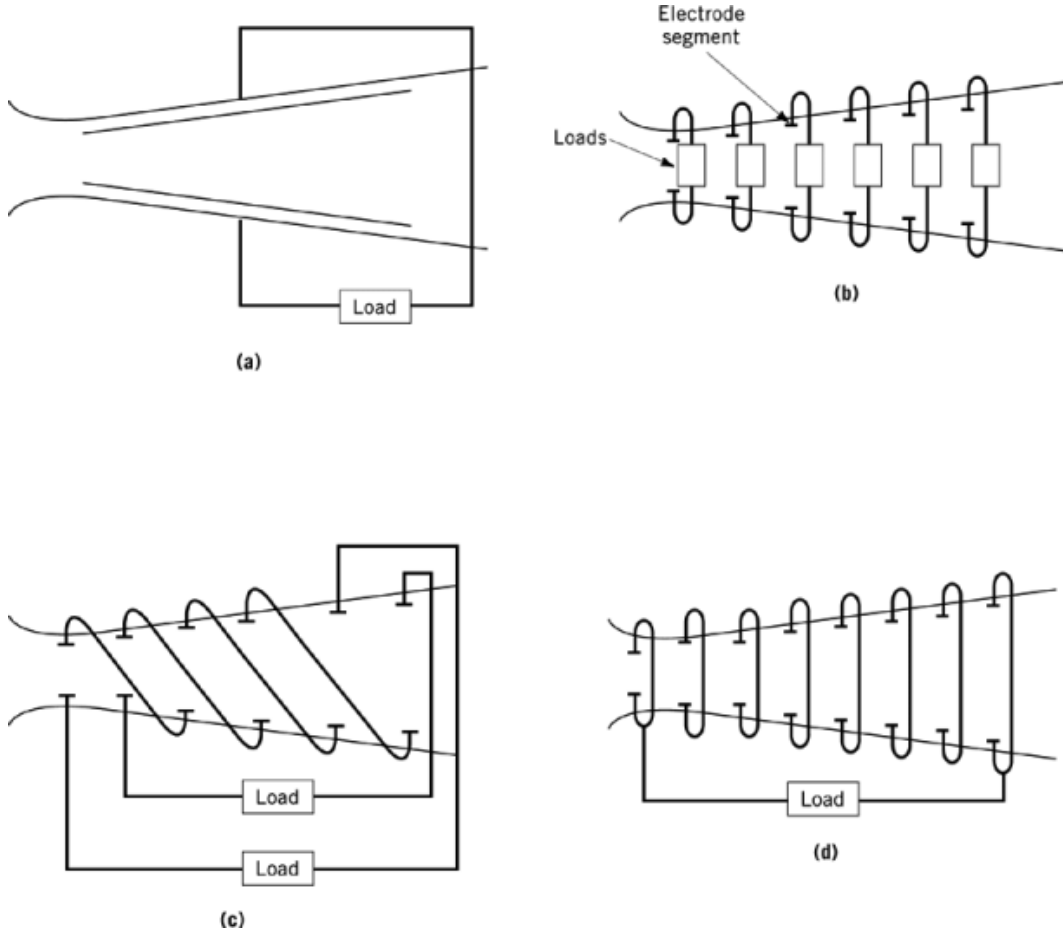


Fig. 5. Linear MHD generator configurations: (a), two-terminal Faraday or continuous electrode; (b), segmented Faraday; (c), diagonal connections; and (d), Hall geometry.

of power collection, in that outputs from several hundred terminals at different potentials must be consolidated into one set of terminals, either at an inverter or at the power grid.

To alleviate these problems, the diagonally connected generator of Figure 5c was devised (23). Those electrodes which would lie at the same potential in a normally operating segmented Faraday generator are connected, ie, the diagonal connection angle $\theta = \tan^{-1} E_y/E_x$. This generator has the advantage of requiring only a few output terminals while in principle operating at conditions which are the same as for the Faraday generator. If the connection angle θ is fixed, the power output and efficiency of the diagonally connected generator equal that of the segmented Faraday generator only at a single operating point, at which $E_y/E_x = \tan \theta$. In fact, E_y and E_x vary as the external load is changed, or as gas conditions change along the channel, and so the ratio E_y/E_x does not remain constant and equal to $\tan \theta$. In principle, performance is degraded as E_y/E_x varies from $\tan \theta$. In practice, generator performance is not extremely sensitive to moderate mismatches between the connection angle and the plasma conditions. The diagonally connected channel design is viewed as an acceptable compromise between optimum performance and mechanical/electrical simplicity. Methods can

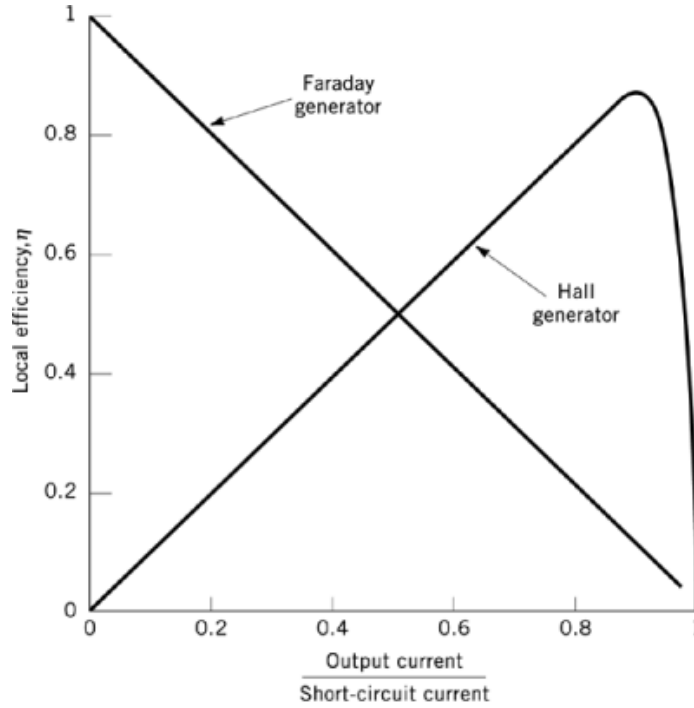


Fig. 6. Local efficiency of Hall and Faraday generators.

be incorporated to change the connection angle to match the changing fields along the channel and to match external load changes, but at the expense of mechanical or electrical complications.

Another configuration having power collection from only two terminals is the Hall generator shown in Figure 5d. In this configuration, opposing electrode pairs are connected, and the current flow for power extraction is axial. $E_y = 0$, and

$$j_x = \frac{\sigma}{1 + \beta^2} (E_x + \beta u B) \quad (30)$$

at open circuit $E_x = -\beta u B$ and so the load parameter in this case is defined as $K' \equiv -E_x / \beta u B$. The power output is

$$P = -j_x E_x = \frac{\beta^2}{1 + \beta^2} K' (1 - K') \sigma u^2 B^2 \quad (31)$$

and the local conversion efficiency is

$$\eta = \frac{\beta^2 K'}{1 + \beta^2 K'} (1 - K') \quad (32)$$

Efficiency and power output approach those of a segmented Faraday generator only for large values of β , $\beta^2 \geq 1$. Figure 6 compares the relative efficiencies of the Hall and segmented Faraday generators. Although the maximum attainable efficiencies are comparable, the highest value in a Hall generator is obtained when the generator is heavily loaded, just the opposite of the situation in a Faraday generator.

12 MAGNETOHYDRODYNAMICS

In a channel operating under power plant conditions, the Hall parameter β varies from about 1 at the channel inlet to about 4 at the channel exit, typically, with an average value of 2–3. This is too high to make the two terminal Faraday configuration attractive, and too low to make the Hall configuration attractive. Thus the segmented Faraday (Fig. 5b) and diagonal geometries (Fig. 5c) are the configurations of choice, and the diagonal configuration is favored because of its simpler electrical loading.

The disk generator, which has certain advantages for particular applications, has also received considerable attention. The disk generator offers a simpler structure, an electrode system having in principle only two electrodes, and a simpler magnet, which has a solenoidal configuration that is easier and less expensive to design and build than the more complex saddle coil configurations required for linear generators. Offsetting these advantages is the disadvantage that a disk generator has a much larger surface-to-volume ratio than a linear generator, and correspondingly larger frictional and heat losses. Thus the disk generator is in principle less efficient than the linear generator and so is less attractive for central station power generation applications. Consequently, the disk generator lags in development status. Nonetheless, it continues to receive attention, primarily for closed cycle power generation (24, 25), but also for open cycle power generation (26, 27).

2.2. Flow and Performance Calculations

Electrodynamic equations are useful when local gas conditions (u , σ , B) are known. In order to describe the behavior of the flow as a whole, however, it is necessary to combine these equations with the appropriate flow conservation and state equations. These last are the mass, momentum, and energy conservation equations, an equation of state for the working fluid, an expression for the electrical conductivity, and the generalized Ohm's law.

The conservation equations are as follows:

$$\text{Mass} \quad \rho u A = \text{constant} \quad (33)$$

$$\text{Momentum} \quad \rho \vec{u} \frac{du}{dx} + \nabla p = \vec{j} \times \vec{B} \quad (34)$$

$$\text{Energy} \quad \rho u \frac{d}{dx} \left(\frac{u^2}{2} + h \right) = \vec{j} \cdot \vec{E} \quad (35)$$

where ρ = density, p = pressure, A = flow cross-section area, and h = specific flow enthalpy. The right-hand term of the momentum equation is a body force, representing the electromagnetic drag force imposed on the flow by the induced currents. The right-hand term of the energy equation is the energy lost from the flow by means of electrical power extraction. The equations of state are

$$p = p(\rho, T)$$

$$h = h(\rho, T) \quad (36)$$

where T = temperature. In addition, a relation for the conductivity σ is necessary:

$$\sigma = \sigma(\rho, T) \quad (37)$$

Relations for transport properties such as viscosity and thermal conductivity are also required if wall friction and heat-transfer effects are considered.

The most widely used approach to channel flow calculations assumes a steady quasi-one-dimensional flow in the channel core, modified to account for boundary layers on the channel walls. Electrode wall and sidewall boundary layers may be treated differently, and the core flow may contain nonuniformities.

In real channels the walls are rough and colder (ca 1700 K), even when covered with slag, than the gas in the bulk of the channel (ca 2500 K). Hence, velocity and thermal boundary layers exist at the channel walls. Their most important effect is to reduce the electrical conductivity at the electrode walls. Resultant voltage losses are caused by the higher electrical resistance of the cold boundary layers through which the induced current must pass. These cold boundary layers also force arc-mode current transport in the coldest regions, as current can no longer traverse in a diffuse mode. Wall friction and heat-transfer effects also exist. In addition, the slag layer on the walls changes the channel geometry somewhat and also allows some electrical leakage.

In the flow models these effects are confined to the boundary layers, maintaining the validity of the quasi-one-dimensional flow model. The flow is generally assumed to be developing, rather than fully developed, and is divided into an inviscid core region occupying most of the channel volume, and boundary layer and slag flow regions confined to the immediate vicinity of the channel walls. The behavior of the boundary layers determines the magnitude of the electrode voltage drops, the heat loss to the walls, the frictional stagnation pressure drop, the potential of axial shorting, the potential for flow separation, etc.

A technique for modeling boundary layers is described in detail in Reference 28. The boundary layer equations are self-consistent and use core flow and wall parameters as boundary conditions. Semiempirical factors are typically introduced to account for wall roughness, axial current leakage along slag layers, core flow nonuniformities, and electrode voltage drops in the presence of arc current transport. MHD effects substantially modify the boundary layer profiles, especially the electrode wall enthalpy profile and the insulating wall velocity profile. Because of the effects of MHD interactions and Prandtl number $\neq 1$, a more general expression between the boundary layer enthalpy and velocity profiles than that given by Crocco's relationship is used. Consequently, the thermal boundary layer and the velocity boundary layer are allowed to develop separately and are not forced to be of equal thickness. The enthalpy distribution affects the electrical conductivity distribution, and, hence, the boundary layer impedance. The conductivity distribution in turn responds to the excessive Joule dissipation near the electrode wall. In the sidewall boundary layers, where the favorable axial pressure gradients are not balanced by the Lorentz force near the wall, the velocity distribution may exhibit overshoot, which may result in negative momentum and displacement thicknesses.

Descriptions of various MHD generator flow models can be found in the literature (28–30). A typical procedure for performing actual channel calculations (29) is to start by specifying the composition of the reactants, from which thermochemical, thermodynamic, and electrical properties of the working fluid are generated (31). The principal input data required to proceed with the calculations are the total mass flow rate, the combustor stagnation pressure and enthalpy, and specified design conditions of magnetic field, electrical load parameter, and Mach number along the channel. It is implicitly assumed that the magnetic field can in fact be treated as a prescribed quantity, ie, it is not significantly influenced by the induced currents in the gas. More sophisticated, two- and three-dimensional computer codes have been developed to treat aspects of channel flow (32, 33). Codes which can treat unsteady flows have also been developed for the analysis of end effects, transient flows, and flows with shock waves, and to determine conditions under which secondary flows or instabilities may occur.

These multidimensional analyses do not necessarily predict overall generator performance or operating characteristics significantly more accurately than do the quasi-one-dimensional analyses, which are more economical to run. Thus the latter are used for general channel design calculations, and the more sophisticated codes mainly to deal with more detailed aspects of channel operation. For example, current concentrations at electrode edges can be predicted by use of the more sophisticated codes. This allows appropriate electrode design for the condition.

14 MAGNETOHYDRODYNAMICS

2.3. Electrical Conductivity

In order to conduct electricity, the working fluid must contain charged particles, ie, it must be partially ionized. Some of the gas atoms or molecules must be stripped of one or more of their electrons. The energy required to accomplish this, called the ionization potential, is measured in electron volts. In MHD flows of interest, the required energy is supplied by heating the gas. Thus the ionization process is referred to as thermal ionization.

Most common gases, eg, air, combustion products such as CO, CO₂, H₂O, and the noble gases, have high (>10 eV) ionization potentials and ionize thermally only at very high (>4000 K) temperatures. Alkali metals, which have much lower (<5 eV) ionization potentials are ionized at much lower temperatures. Thus small amounts (~1%) of alkali metal salts are added to a gas at typical combustion temperatures (2500–3000 K) and enough ionization is obtained to achieve usable levels of electrical conductivity. This process is called seeding, and is a practical way of obtaining useful conductivities at temperatures that can be withstood in practical devices. The seed material used in MHD generators is most commonly a potassium salt, eg, potassium carbonate or potassium formate, both of which are readily available and economical. Cesium salts, which have an even lower ionization potential, are sometimes used when maximum conductivity is necessary, but are not economical for power plant use. Electrical conductivities in potassium-seeded combustion gases are in the range 1 – 10 mho/m.

The electrical conductivity σ of a gas is defined as the ratio of the current to the field, ie, from the most general form of Ohm's law. Neglecting ion mobility, this becomes equation 16, which can be written in terms of the current density components:

$$\begin{aligned}\vec{j}_x &= \sigma \vec{E}_x'' - \frac{\beta}{B} (j_y B_z - j_z B_y) \\ \vec{j}_y &= \sigma \vec{E}_y'' - \frac{\beta}{B} (j_z B_x - j_x B_z) \\ \vec{j}_z &= \sigma \vec{E}_z'' - \frac{\beta}{B} (j_x B_y - j_y B_x)\end{aligned}\quad (38)$$

If the magnetic field is in the z direction, $B_z = B$ and $B_x = B_y = 0$, $E_z'' = 0$. Solving for the current density components:

$$\begin{aligned}j_x &= \sigma E_x'' - \frac{\sigma\beta}{1 + \beta^2} E_y'' \\ j_y &= \frac{\sigma}{1 + \beta^2} E_y'' + \frac{\sigma\beta}{1 + \beta^2} E_x'' \\ j_z &= 0\end{aligned}\quad (39)$$

Equations 39 have the form

$$j_i = \sum_{k=1}^3 \sigma_{ik} E_k'' \quad (40)$$

where the conductivity σ_{ik} is a tensor quantity the value of which depends on the magnetic field and on the orientation of the electric field to the magnetic field. If an electric field is aligned with the magnetic field, ie, in the z -direction, then $E'' = E_z''$ and $E_x'' = E_y'' = 0$. Then $j_x = j_y = 0$; $j_z = \sigma E_z''$ and the current density has the same direction as, and is proportional to, the electric field. The conductivity is independent of the magnetic

field strength and is called the scalar conductivity. This is the conductivity of the plasma in the absence of a magnetic field (see Plasma technology).

When the electric field is not aligned with the magnetic field, the conductivity is not independent of the magnetic field. For example, if the total electric field E' is perpendicular to the magnetic field, in the y -direction, then $E'' = E'_y$ and $E'_x = E'_z = 0$. Then equations 39 become

$$j_x = -\frac{\sigma\beta}{1+\beta^2}E''_y$$

$$j_y = \frac{\sigma}{1+\beta^2}E''_y \quad (41)$$

$$j_z = 0$$

Now the effective conductivity in the direction of the electric field is $\sigma/(1+\beta^2)$, ie, the scalar conductivity reduced by a factor of $(1+\beta^2)$ by the magnetic field. Also, the electric current no longer flows in the direction of the electric field; a component j_x exists which is perpendicular to both the electric and magnetic fields. This is the Hall current. The conductivity in the direction of the Hall current is greater by a factor of β than the conductivity in the direction of the electric field. The calculation of the scalar conductivity starts from its definition:

$$\sigma = \frac{j}{E} \quad (42)$$

where j is the total conduction current

$$j = \sum_k n_k v_k Z_k e \quad (43)$$

The subscript k identifies the different species present, n_k is the number density of the k^{th} species, v_k its drift velocity, and Z_k denotes the number of charges on a particle of species k ,

$$n_k v_k = \int c f_k dc \quad (44)$$

where c is the random thermal speed of the particle and f_k is the distribution function of the k^{th} species.

In order to calculate $n_k v_k$, the distribution function f_k must be obtained in terms of local gas properties, electric and magnetic fields, etc, by direct solution of the Boltzmann equation. One such Boltzmann equation exists for each species in the gas, resulting in the need to solve many Boltzmann equations with as many unknowns. This is not possible in practice. Instead, a number of expressions are derived, using different simplifying assumptions and with varying degrees of validity. A more complete discussion can be found in Reference 34.

A relatively simple derivation assumes that the current is carried primarily by electrons. Then equation 43 becomes equation 13, $j_e = n_e v_e e$, where v_e is the electron drift velocity. An electron with charge e in an electric field E experiences a force eE in the direction of the field, and an acceleration eE/m_e , where m_e is the electron mass. The electron also has a random thermal motion which causes it to collide with the other particles in the gas. Assuming that the electron drifts with its field-induced drift velocity, v_e , only between collisions,

16 MAGNETOHYDRODYNAMICS

then

$$v_e = \left(\frac{Ee}{m_e} \right) \tau \quad (45)$$

where τ is the mean free time between collisions. This assumes that on each collision the electron loses all the directed motion acquired from the field. The mean free time between collisions is given by

$$\tau = 1/nQc_e \quad (46)$$

where n is the number density of atoms or molecules in the gas, Q their momentum transfer cross section, and c_e the mean random thermal speed of the electrons. Combining equations 43–46,

$$\sigma = \frac{n_e e^2}{m_e n Q c_e} \quad (47)$$

Only the quantities n_e , the electron number density, and Q , the collision cross section, present any difficulty in their calculation.

To calculate n_e , electron production must be balanced against electron depletion. Free electrons in the gas can become attached to any of a number of species in a combustion gas which have reasonably large electron affinities and which can readily capture electrons to form negative ions. In a combustion gas, such species include OH (1.83 eV), O (1.46 eV), NO₂ (3.68 eV), NO (0.09 eV), and others. Because of its relatively high concentration, its ability to capture electrons, and thus its ability to reduce the electrical conductivity of the gas, the most important negative ion is usually OH[−].

Assuming that the gas is electrically neutral over regions having dimensions larger than the Debye length, typically of the order 10^{-6} m in an MHD generator, the electron and ion densities in the bulk of the gas are equal.

The mass action law or Saha equation for thermal ionization of seed atoms is

$$\frac{n_e n_i}{n} = \frac{(2\pi m_e kT)^{3/2}}{h^3} \frac{2g_i}{g_0} \exp\left(-\frac{e\epsilon_i}{kT}\right) \quad (48)$$

where n_i = ion concentration, n = neutral seed atom concentration, h = Planck's constant, ϵ_i = ionization potential of seed atom, g_i = the statistical weight of the ground state of the ion, and g_0 = the statistical weight of the ground state of the neutral atom (35).

The quantities g_i and g_0 that appear in equation 48 are approximations for the complete partition function. For highest accuracy, above about 9000 K, the partition functions should be used.

A form of equation 48 which can be conveniently expressed in terms of equilibrium constants is

$$\log \frac{n_e n_i}{n_0 - n_i} = \frac{-5,040}{T} \epsilon_i - \frac{3}{2} \log \frac{5,040}{T} + 26.9366 + \log \frac{2g_i}{g_0} \quad (49)$$

where n_0 is the original concentration of seed atoms before ionization.

A derivation of equation 49 is given in Reference 36. In flows of interest in MHD power generation the total pressure is about 101 kPa (1 atm) and the partial pressure of seed is 1 kPa (0.01 atm). Also, it is usually possible to assume that $n_e = n_i$ and that only one species (seed atoms) ionize. In rare situations, more than one species may ionize, if so, equation 49 must be solved simultaneously for each species with the constraint that $n_e = n_{i1} + n_{i2} + \dots + n_{in}$.

Referring back to equation 47, the other quantity necessary in calculating the gas conductivity is the collision cross section, Q . Gases contain at least four types of particles: electrons, ionized seed atoms, neutral seed atoms, and neutral atoms of the carrier gas. Combustion gases, of course, have many more species. Each species has a different momentum transfer cross section for collisions with electrons. To account for this, the product nQ in equation 47 is replaced by the summation $\sum_k n_k Q_k$ where k denotes the different species present. This generalization also allows the conductivity calculation to include the total current in the gas, obtained from the summation of the currents carried by each type of charged particle. A separate term accounting for electron-ion collisions is added, as ions have a very large cross section for collisions with electrons owing to the Coulombic field which surrounds them. Including the term for electron-ion cross sections, the expression for conductivity becomes

$$\sigma = \frac{n_e e^2}{m_e c_e} \left[\frac{1}{\sum_k n_k Q_k + 3.9 n_i \left(\frac{e^2}{8\pi \epsilon_0 k T} \right)^2 \ln \Lambda} \right] \quad (50)$$

where the summation over k includes all species except for ions, which are accounted for in the second term in the denominator (35).

Other quantities in equation 50 are ϵ_0 = permittivity of free space, and

$$\Lambda = \frac{12\pi}{n_e} \left(\frac{\epsilon_0 k T}{e^2} \right)^{3/2} \quad (51)$$

Equation 50 is adequate in most cases, but becomes inaccurate if the collision cross sections are strongly temperature dependent. In this case, integral expressions for cross section are necessary, and the expression for conductivity becomes more complicated, eg,

$$\sigma = \frac{4\pi}{3} \frac{n_e}{n_k} \frac{e^2}{k T_k} \left(\frac{m_e}{2\pi k T_k} \right)^{3/2} \int \frac{c_e^3}{Q_{ek}} e^{-m_e c_e^2 / 2k T_k} d c_e \quad (52)$$

The collision cross sections are functions of the electron energy and of the relationship which describes the forces between the heavy particles and the electrons (34).

A widely used method for calculating conductivity (37), uses the relationship between conductivity and electron mobility given by equation 14, $\sigma = n_e \mu_e e$. The electron mobility (38) is given by

$$\mu_e = -\frac{4\pi e}{3m_e} \int_0^\infty \frac{u^3}{v} \cdot \frac{d}{dv} f(v) dv \quad (53)$$

18 MAGNETOHYDRODYNAMICS

where $f(v)$ is the electron velocity distribution function,

$$f(v) = \left(\frac{m_e}{2\pi kT} \right)^{\frac{3}{2}} \exp \left(\frac{-m_e v^2}{2kT} \right) \quad (54)$$

The collision frequency, ν_k , for momentum transfer with a particular molecular or atomic species, k , is given by

$$\nu_k = \nu_e n_k Q_k \quad (55)$$

and the total collision frequency with all neutral species is $\nu_0 = \sum \nu_k$. If electron-ion collisions are also accounted for, with ν_{ei} being the electron-ion collision frequency, the total collision frequency ν is

$$\nu = \sum \nu_k + \nu_{ei} \quad (56)$$

The electron-ion collision frequency can be approximated by the Spitzer-Harm (39) formulation for a completely ionized gas:

$$\nu_{ei} = \frac{3.64 \times 10^6}{T^{1.5}} n_e \ln \left[\left(1.27 \times 10^7 \right) T^{1.5} / n_e^{0.5} \right] \quad (57)$$

Electron-ion collisions become important when the degree of ionization exceeds about 0.1% and introduce additional complexity in calculating their effects. Methods for calculating conductivity in strongly ionized gases are given in Reference 40.

To evaluate the mobility, the reciprocal of the collision frequency is expressed as a power series in electron energy, allowing the integration in equation 53 to be performed analytically.

Conductivity is calculated according to equation 14 by combining the mobility results with the electron density obtained as described earlier. Results for the combustion products typical of a coal-fired MHD generator are shown in Figure 7. A very strong dependence on temperature can be seen. At a seed concentration of 1.2% by weight of potassium, the conductivity is about 8 mho/m at typical generator temperatures of 2500 K, whereas at 2300 K it has dropped to about 2 mho/m, a value too low to be useful for power generation. This reflects the temperature dependence of electron number density. The conductivity is not so sensitive to changes in seed concentration, varying only about 10% over a factor of three range in potassium concentration. This is because of the increase in the cross section and number density of KOH molecules as the potassium concentration is increased.

3. Efficiency and Economic Factors

Because the MHD generator has no moving mechanical parts, it can operate at a much higher combustion temperature than other power generating systems, allowing the combined MHD-steam cycle to achieve higher thermal efficiency than other systems. The high efficiencies together with competitive capital costs yield very attractive cost of electricity (COE) estimates for MHD. A comparison of about 20 advanced technology processes with a conventional steam plant (41, 42) concluded that the coal-fired open-cycle MHD system has potentially one of the highest coal pile-to-busbar efficiencies as well as one of the lowest COEs among the systems studied. Figure 8 summarizes COE comparisons for a number of advanced power cycles (43). The cost of electricity was found to be lower for MHD than for any other advanced coal-fueled power system studied. The COE is about 25% lower for MHD than for a modern steam plant at a coal cost of \$20/t (\$0.97/MBtu) in 1978 dollars.

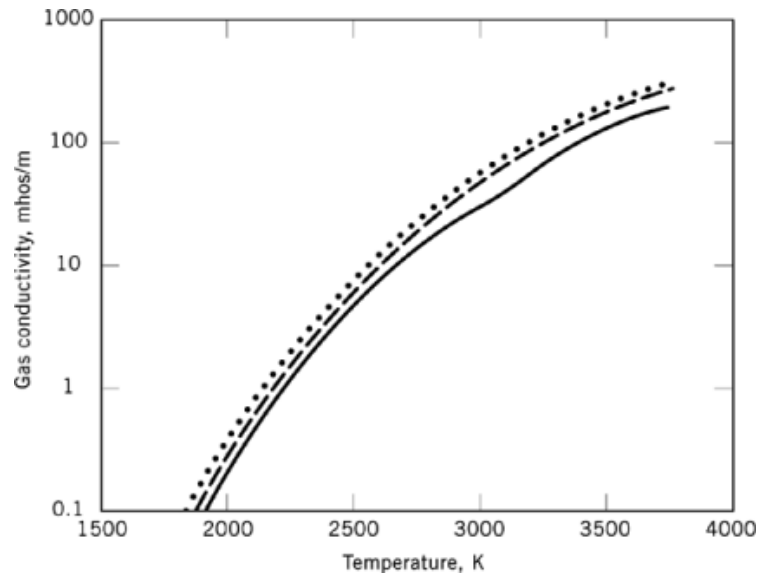


Fig. 7. Electrical conductivity of combustion products where the fuel is Montana subbituminous coal, the oxidizer, $\text{air} + \text{O}_2$, having a fuel:oxidizer stoichiometric ratio of N:O 0.65; and the pressure, 101 kPa (1 atm). (—), (—), and (...) represent 0.5, 1.2, and 1.6 wt%potassium, respectively.

Higher thermal efficiency and the corresponding smaller influence of fuel cost leads to the COE advantage of MHD increasing as the cost of fuel increases. Studies summarized in Table 1 (44–46), predict that first generation MHD–steam power plants should have thermal efficiencies in the 42% range and as the technology matures, plant efficiency should increase to 55–60%. This may be compared with 33–38% for modern coal-fired steam plants having scrubbers. The first commercial MHD plants shown in Table 1 are to use oxygen-enriched air at a moderate (922 K) preheat temperature as the oxidant, and are 40–42% efficient (44). Conceptual design studies using economic analysis have shown that such first generation MHD power plants are economically attractive (44, 45). The advanced MHD plant of the future (46) should achieve an efficiency of 58% mainly because it uses high temperature (1978 K) air heaters fired directly by the channel exhaust gas instead of oxygen enrichment, and has a more advanced topping cycle, a higher magnetic field, and a more highly stressed channel. This last plant operates at higher pressure and has improvements in other parts of the cycle.

4. Environmental Factors

Environmental intrusion from MHD plants is projected to be not only well below the mid-1990s acceptable limits, but also low enough to satisfy the more stringent requirements expected in the future. Emissions of SO_x , NO_x , and particulates can be reduced to levels well below the 1979 NSPS without requiring expensive exhaust gas cleanup systems. Pollutant control is inherent in the basic design of MHD power plants. Furthermore, because of the higher efficiency and consequent lower fuel usage of MHD plants, emissions of CO_2 are lower, heat rejection is reduced, and less solid waste is produced than from other less efficient plants. Table 2 (46) compares a mature MHD–steam power plant to a conventional plant. Emissions are lower from the MHD plants because of MHD's lower fuel usage.

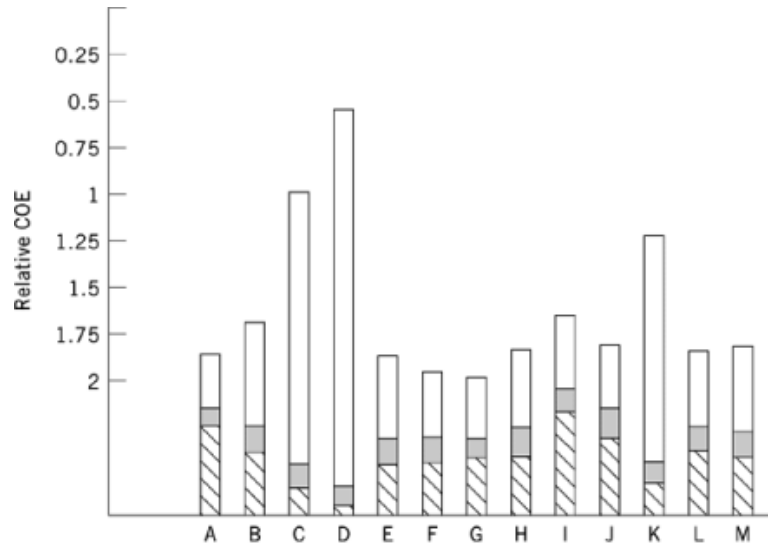
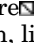
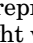
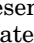
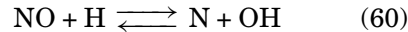
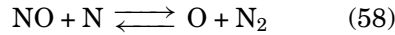


Fig. 8. Cost of electricity (COE) comparison where  represents capital charges,  operation and maintenance charges, and  fuel charges for the reference cycles, A, steam, light water reactor (LWR), uranium; B, steam, conventional furnace, scrubber coal; C, gas turbine combined cycle, semiclean liquid; D, gas turbine, semiclean liquid, and advanced cycles; E, steam atmospheric fluidized bed, coal; F, gas turbine (water-cooled) combined low heating value (LHV) gas; G, open cycle MHD coal; H, steam, pressurized fluidized bed, coal; I, closed cycle helium gas turbine, atmospheric fluidized bed (AFB), coal; J, metal vapor topping cycle, pressurized fluidized bed (PFB), coal; K, gas turbine (water-cooled) combined, semiclean liquid; L, gas turbine (air-cooled) combined, LHV gas; M, steam (650°C reheat), AFB coal.

At the high temperatures found in MHD combustors, nitrogen oxides, NO_x , are formed primarily by gas-phase reactions, rather than from fuel-bound nitrogen. The principal constituent is nitric oxide [10102-43-9], NO , and the amount formed is generally limited by kinetics. Equilibrium values are reached only at very high temperatures. NO decomposes as the gas cools, at a rate which decreases with temperature. If the combustion gas cools too rapidly after the MHD channel the NO has insufficient time to decompose and excessive amounts can be released to the atmosphere. Below about 1800 K there is essentially no thermal decomposition of NO .

Reactions of primary interest during the cooling process are as follows:



where equations 58 and 59 are the well-known Zeldovich reactions (47) and equation 60 is of particular interest in fuel-rich mixtures typical of MHD flows. Although these three are the dominant reactions, there are a large number of other reactions and species which can influence NO decomposition (48). Detailed studies of NO decomposition, both analytical and experimental, are described in the literature (49–52).

Table 1. Comparison of MHD and Conventional Steam Plants^a

Type of cycle	Conventional pulverized coal steam	MHD steam	
		First commercial	Advanced direct-fired
net plant output, MW _e	954	212–492	953
net plant efficiency, ^b %	37.4 ^c	40.2–41.7	58.1
combustor oxidant	air	air + oxygen ^d	air
air heater type	Lungstrom-type regenerative	recuperative metal	direct-fired regen-erative refractory
combustion air preheat, K	589	922	1978
combustion pressure, kPa ^e	101	555	1460
MHD stress level	none	POC ^f	advanced
steam cycle:	current	current	current
throttle pressure, MPa ^e	24.0	16.5	24.0
outlet temperatures, K			
superheater	811	811	811
first reheat	839	811	839
second reheat	none	none	none

^aPrimary fuel for each plant is pulverized Illinois No. 6 coal.^bOn a higher heating value basis.^cObtainable only in modern plants. Average for U.S. plants is 32.8%.^dTotal oxygen concentration is 32 mol%.^eTo convert kPa to psi, multiply by 0.145.^fSimilar to levels planned for proof of concept (POC) tests.**Table 2. Environmental Intrusion Comparison^a**

Parameter	Conventional steam power plant	MHD–steam power plant	
		Early	Advanced
carbon dioxide, kg	844	703	522
solid wastes, kg	116	98	748
cooling tower heat rejection, GJ ^b	4.511	3.43	1.67
cooling water consumption, kg	2176	1436	905

^aAll data are per megawat-hour.^bTo convert GJ to millions of Btu, multiply by 0.9485.

NO_x control is achieved by means of a two-stage combustion process. Primary combustion occurs in the coal combustor under fuel-rich conditions. Secondary combustion takes place in the heat recovery boiler after cooling the fuel-rich MHD generator exhaust gases in a radiant furnace which provides a residence time of at least two seconds at a temperature above 1800 K. Conditions in the radiant furnace allow the NO to decompose into N₂ and O₂. The cooling rate of the exhaust gas is the key element in the decomposition. The required residence time is provided by appropriate design of the radiant furnace. Using proper choices of primary stoichiometry, gas cooling rates, and secondary combustion temperatures, NO_x emissions are kept below the proposed European standard of 0.04 kg/GJ (0.1 lb/(Btu × 10⁶)), as shown in Figure 9 (53).

Control of SO_x is intrinsic to the MHD process because of the strong chemical affinity of the potassium seed in the flow for the sulfur in the gas. Although the system is operated fuel-rich from the primary combustor to the secondary combustor, the predominant sulfur compound in the gas is sulfur dioxide (54, 55). Hydrogen sulfide begins to form at gas temperatures below about 2000 K and about 10 mol % of the sulfur is present as H₂S at 1800 K. At lower temperatures SO₂ converts rapidly to H₂S. The primary factor affecting SO₂

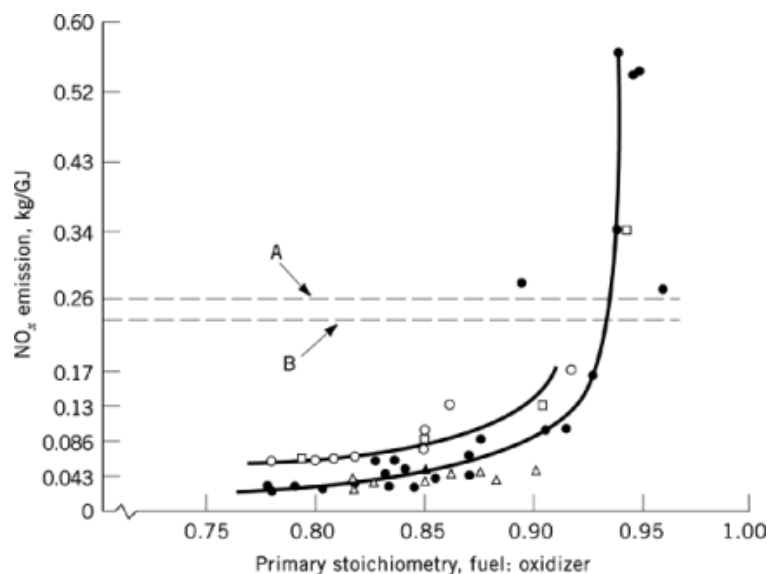


Fig. 9. Measured coal-fired flow facility (CFFF) NO_x emissions where (●) represents high sulfur coal, (○) low sulfur coal, (△) low sulfur coal having $K_2/S=1.15$, and (□) LMF5-G. A, Illinois No. 6 coal (3%S); B, Montana Rosebud coal (1%S), and the NSPS range is between the dotted lines. To convert kg/GJ to lb/(MBtu) , multiply by 2.326.

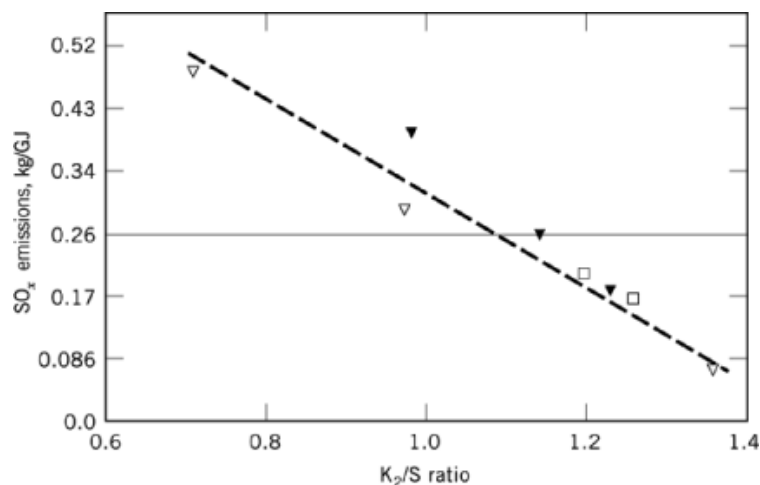


Fig. 10. Effect of potassium on SO_2 removal where (—) represents the NSPS limit, and (▽) represents LMF4-T, (▼) LMF4-U, and (□) LMF4-V.

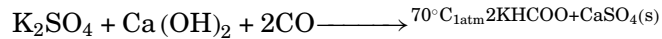
removal is the potassium to sulfur molar ratio. At K_2/S ratios >1.4 , SO_2 emissions are reduced to $<0.04 \text{ kg/GJ}$ (0.1 lb/MBtu) (see Fig. 10) (53).

The potassium combines with the sulfur to form potassium sulfate, which condenses as a solid primarily in the electrostatic precipitator (ESP) or baghouse. The recovered potassium sulfate is then delivered to a seed regeneration unit where the ash and sulfur are removed, and the potassium, in a sulfur-free form such as formate or carbonate, is recycled to the MHD combustor. It is necessary also to remove anions such as Cl^- and

F⁻ which reduce the electrical conductivity of the generator gas flow. These are present in the coal ash in very small and therefore relatively harmless concentrations. As the seed is recycled, however, the concentrations, particularly of Cl⁻, tend to build up and to become a serious contaminant unless removed.

Several methods for reprocessing the potassium seed have been considered, including the double alkali process, the Engle-Precht process, the aqueous carbonate process, the Pittsburgh Energy Technology Center (PETC, U.S. Dept. of Energy) process, and the formate process, among others. A review (56) and more detailed descriptions of some of the processes are available (57–60).

Considerable attention has been given to the formate process where the primary reaction is



A diagram for one implementation of this process (61, 62) is shown in Figure 11. Recovered potassium sulfate is converted to potassium formate [590-29-4] by reaction with calcium formate [544-17-2], which is made by reacting hydrated lime, Ca(OH)₂, and carbon monoxide. The potassium formate (mp 167°C), in liquid form, is recycled to the combustor at about 170°C. Sulfur is removed as solid calcium sulfate by filtration and then disposed of (see Sulfur removal and recovery).

The cost penalty of this process on a commercial MHD plant operating on a high sulfur eastern coal is estimated to be in the range \$0.0154 – 0.0181/kWh, depending on seed loading. For a plant operating on a low sulfur western coal the cost penalty is estimated to be in the range \$0.0068 – 0.0112/kWh (62). A resin-based anion-exchange seed regeneration process has been suggested (60), which promises considerable process simplicity, less Cl⁻ contamination, and lower costs.

Particulates in the MHD exhaust gas stream are primarily (80–90%) K₂SO₄, the remainder being coal ash constituents. Because of the very high temperatures in the MHD combustor, most of the particles have undergone vaporization and condensation steps. Most of the slag is rejected into a slag tap upon entering the radiant furnace. The remaining slag forms particles, primarily, it is believed, by homogeneous nucleation. The potassium compounds form particles by both homogeneous and heterogeneous nucleation, with the condensed ash particles serving as nucleation sites for the heterogeneous nucleation. Because of the high combustion temperatures and the presence of a lower boiling species (potassium), MHD systems produce very small particles. The average mass mean diameter varies between 0.2 μm at K₂/S ratios near 1 and 0.7 μm at K₂/S ratios near 4. This is almost two orders of magnitude smaller than those found in typical utility operation. The particle size distribution appears to be unaffected by the type of coal used. Particulate mass loadings are in the range 11–18 g/m³ (5–8 grains per dry standard cubic foot). The most commonly used particulate collection device on coal-fired power plants is the dry electrostatic precipitator (ESP). Because of the presence of potassium salts in the particulate, the resistivity is typically 10⁹ Ω·cm, regardless of coal type. Thus ESP problems associated with high resistivity do not occur in MHD systems. Requirements set by NSPS are met or exceeded (53), although the specific collection area required for MHD may be somewhat higher than for conventional systems. Particulate collection performance using a baghouse has been measured at 0.0013 – 0.026 kg/GJ (0.003 – 0.006 lb/MBtu (53), well below NSPS limits (0.13 kg/GJ). Because of the submicrometer particulates, Gore-tex bag material may be necessary to eliminate the effects of fabric blinding.

The high temperatures in the MHD combustion system mean that no complex organic compounds should be present in the combustion products. Gas chromatograph/mass spectrometer analysis of radiant furnace slag and ESP/baghouse composite, down to the part per billion level, confirms this belief (53). With respect to inorganic priority pollutants, except for mercury, concentrations in MHD-derived fly-ash are expected to be lower than from conventional coal-fired plants. More complete discussion of this topic can be found in References 53 and 63.

24 MAGNETOHYDRODYNAMICS

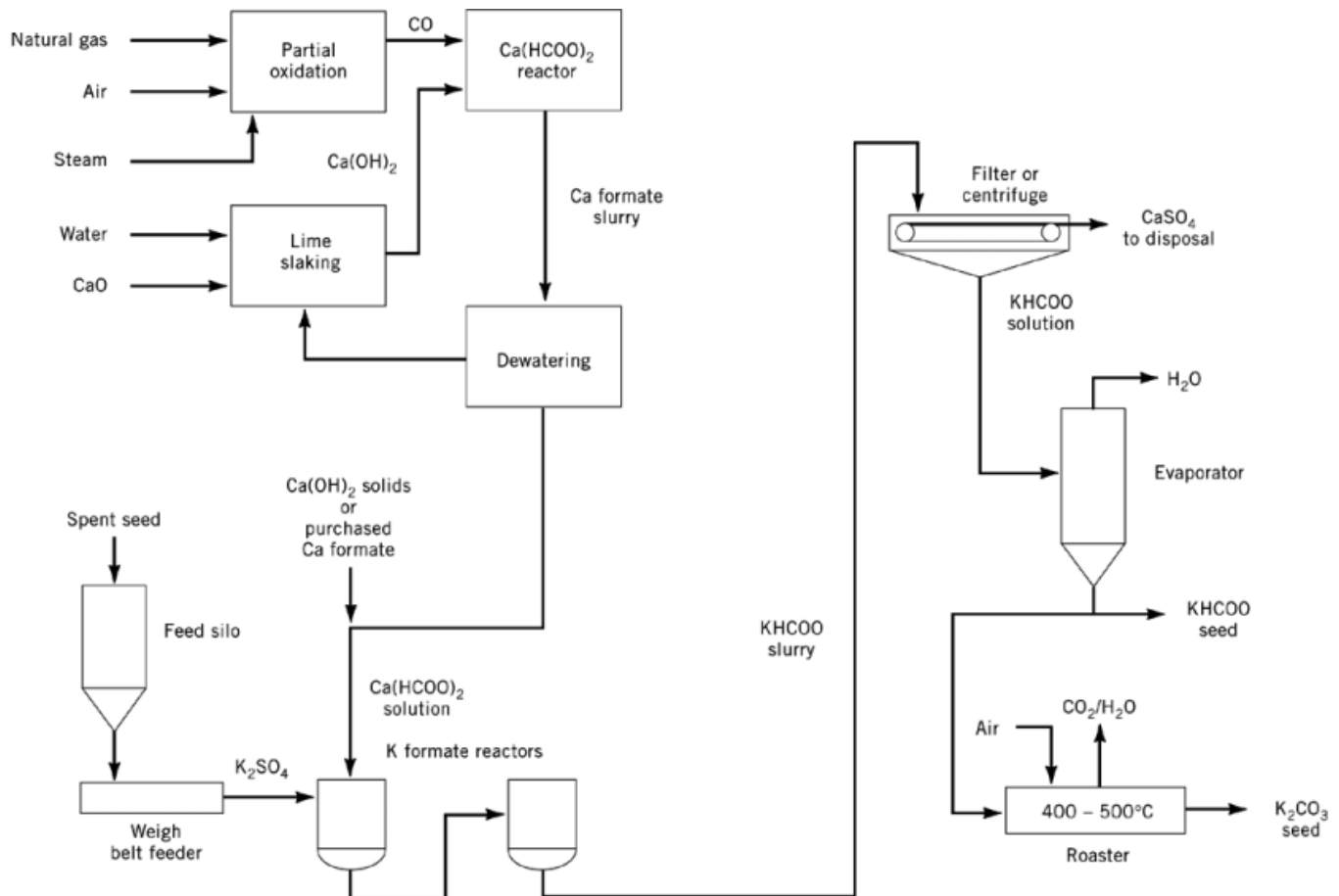


Fig. 11. TRW, Inc. econoseed process where the reactor in the first step is at a pressure from 8.3–8.9 MPa (1200–1290 psi) and 150–200°C.

5. Power Plants

A complete MHD power plant must integrate the MHD generator and the bottoming plant to maximize plant efficiency and minimize cost of electricity. Net plant efficiency is maximized by simultaneous optimization of net MHD power generation, ie, MHD generator power minus the cycle compressor power and oxygen plant compressor power, and of waste heat utilization in the steam bottoming plant. Compromises between performance and cost, particularly of the magnet but also of the oxygen plant and other ancillary equipment, must be made.

Power system designs and analyses have been performed on both stand-alone MHD-steam plants (44, 46, 64), and on retrofit plants (65). These latter are MHD topping cycles retrofitted to existing steam plants. In a first generation commercial MHD power plant producing 500 MW of electricity, and operating on Montana subbituminous coal, approximately half (261 MW) of the total plant output would be produced by the MHD channel (44). Overall design parameters are as follows: for MHD combustion, oxidizer O_2 content, 34 vol %; fuel moisture as fired, 5%; ash slag removal, 80%; oxidizer/fuel equivalence ratio, 0.90; and combustor coolant, high pressure boiling feed water. The MHD generator is a diagonal channel type having subsonic channel gas

velocity and a peak magnetic field of ca -6 T ($6 \times 10^4 \text{ G}$); the gas seed concentration is 1.0% potassium and the seed regeneration process a formate one; the diffuser recovery factor, 0.6; the diffuser exit pressure 101 kPa (1.0 atm); and the channel coolant, low pressure boiler feed water. For the bottoming plant: the main steam is at 16.5 MPa (163 atm) at 807 K; the reheat steam at 807 K. The final MHD combustor gas O_2/fuel equivalence ratio is 1.05. The operating pressure ratio of the plant is 7.5. The net plant efficiency is 42.9% from the coal pile to busbar. The plant utilizes oxygen-enriched (34 vol % oxygen) combustion air preheated to 922 K in a metallic, recuperative-type, tubular heat exchanger which is part of the bottoming plant heat recovery system. The oxygen is produced at a purity of 80%, in an oxygen plant which is integrated with the power plant.

The Rankine cycle efficiency of the bottoming plant is 41.6%. To utilize the waste heat from the topping cycle, low pressure and low temperature feedwater is used for channel cooling, and high pressure and high temperature feedwater for cooling of the MHD combustor. The total feedwater temperature rise in the feedwater heater train is 178°C for the plant, which employs a total of six heaters. Cooling of the diffuser is incorporated as part of the evaporative circuit of the steam cycle. Heat recovered from the hot MHD generator exhaust gas is used for steam generation, oxidizer preheating to 922 K, feedwater heating in a split high pressure (HP) and low pressure (LP) economizer, coal drying, and preheating of secondary combustion air to 589 K. The secondary combustion air is introduced into the bottoming plant steam generator for afterburning, in order to achieve final oxidation of the fuel-rich MHD combustion gases. Flue gas at stack gas temperature is also utilized for spray drying in the seed regeneration system for effective utilization of waste heat.

The oxygen plant delivers 3996 t/d of contained oxygen at full load. The specific compressor power required for manufacturing of oxygen is 190 kWh/t of contained oxygen (or 203.5 kWh/t of equivalent pure oxygen), corresponding to 31.6 MW_e at nominal plant load conditions. The required compressor power for oxygen manufacturing is provided by steam turbines which are part of the bottoming plant steam cycle. High pressure steam is used for the turbine which drives the cycle compressor and oxygen plant compressor.

The resulting overall energy balance for the plant at nominal load conditions is shown in Table 3. The primary combustor operates at 760 kPa (7.5 atm) pressure; the equivalence ratio is 0.9; the heat loss is about 3.5%. The channel operates in the subsonic mode, in a peak magnetic field of 6 T. All critical electrical and gas dynamic operating parameters of the channel are within prescribed constraints; the magnetic field and electrical loading are tailored to limit the maximum axial electrical field to 2 kV/m, the transverse current density to 0.9 A/cm^2 , and the Hall parameter to 4. The diffuser pressure recovery factor is 0.6.

The channel length is 18 m, having a cross section of about $0.7 \times 0.7 \text{ m}^2$ at the inlet and $1.8 \times 1.8 \text{ m}^2$ at the exit. Channel performance (net MHD power, enthalpy extraction) could be improved by increasing the oxygen enrichment and the channel length. However, the overall system would then be penalized by the increased oxygen plant costs, from the increased oxygen enrichment; by higher magnet costs, from the increased channel length; and by the adverse impact on waste heat recovery and steam plant efficiency from increased channel heat loss. The channel cooling is limited to low temperature and low pressure feedwater in accordance with state-of-the-art channel technology.

An alternative configuration which could be considered is a supersonic channel in a lower (4–4.5 T) magnetic field. This configuration would suffer a relatively small penalty in MHD generator performance and net power output, but the magnet would be considerably smaller, having stored magnetic energy of half or less of that at subsonic operation. Thus, there is a significant reduction in magnet cost and risk to be weighed against the relatively small reduction in plant performance. The oxygen plant required for supersonic operation is somewhat larger than that required for subsonic operation, which increases its cost.

The plant is designed to satisfy NSPS requirements. NO_x emission control is obtained by fuel-rich combustion in the MHD burner and final oxidation of the gas by secondary combustion in the bottoming heat recovery plant. Sulfur removal from MHD combustion gases is combined with seed recovery and necessary processing of recovered seed before recycling.

The steam generator is a balanced draft, controlled circulation, multichamber unit which incorporates NO_x control and final burnout of the fuel-rich MHD combustion gases. The MHD generator exhaust is cooled

Table 3. Overall Energy Balance at 500 MW_e Nominal Load

Parameter	Value, MW
<i>Fuel input</i>	
MHD combustor	1162.0
gasifier for seed regeneration	16.0
<i>Total</i>	<i>1178.0</i>
<i>Gross power outputs</i>	
MHD power	261.0
steam power ^a	359.6
<i>Total</i>	<i>620.6</i>
<i>Auxiliary and losses</i>	
cycle compressor	57.7
O ₂ plant compressor	31.6
auxiliaries	19.5
inverter and transformer	7.7
<i>Total</i>	<i>116.5</i>
net plant output	504.1
net plant efficiency,%	42.9 ^b

^aIncludes power from recovery of available heat in seed system.

^bThis number is a percentage.

in a primary radiant chamber from about 2310 to 1860 K in two seconds, and secondary air for afterburning and final oxidation of the gas is introduced in the secondary chamber where seed also condenses. Subsequent to afterburning and after the gas has been cooled down sufficiently to solidify condensed seed in the gas, the gas passes through the remaining convective sections of the heat recovery system.

The oxidant preheater, positioned in the convective section and designed to preheat the oxygen-enriched air for the MHD combustor to 922 K, is located after the finishing superheat and reheat sections. Seed is removed from the stack gas by electrostatic precipitation before the gas is emitted to the atmosphere. The recovered seed is recycled by use of the formate process. Alkali carbonates are separated from potassium sulfate before conversion of potassium sulfate to potassium formate. Sodium carbonate and potassium carbonate are further separated to avoid buildup of sodium in the system by recycling of seed. The slag and fly-ash removed from the HRSR system is assumed to contain 15–17% of potassium as K₂O, dissolved in ash and not recoverable.

The basic seed processing plant design is based on 70% removal of the sulfur contained in the coal used (Montana Rosebud), which satisfies NSPS requirements. Virtually complete sulfur removal appears to be feasible and can be considered as a design alternative to minimize potential corrosion problems related to sulfur in the gas. The estimated reduction in plant performance for complete removal is on the order of 1/4 percentage point. The size of the seed processing plant would have to be increased by roughly 40% but the corresponding additional cost appears tolerable. The construction time for the 500 MW_e plant is estimated to be ca five years.

In a more advanced MHD-steam plant (46), the main difference is the use of 1978 K air preheat, achieved by means of a regenerative air preheater fired directly by the exhaust gases from the MHD diffuser. No oxygen enrichment is used. Other differences are the use of a supercritical steam cycle, a higher peak magnetic field (10 T) and a channel operating at higher electrical fields and currents. For Illinois No. 6 coal as fuel, the net plant output is projected to be 953 MW for a net efficiency of 58.1%. Operating parameters are shown in Table 4.

Table 4. Advanced MHD Topping Cycle Parameters^a

Parameter	Value
coal thermal (HHV) input, ^b MW _t	1641
combustion air preheat, K	1978
inlet total pressure, MPa ^c	1.47
combustor stoichiometry	0.90
seed,% potassium	1.0
combustor exit flow, kg/s	545.9
exit total temperature, K	2941
inlet	
Mach number	0.95
static temperature, K	2768
static pressure, MPa ^c	0.885
conductivity, (Ω·m ⁻¹)	7.63
channel ^d length, m	26.7
inlet area, m ²	0.533
exit area, m ²	7.457
maximum magnetic field, T	10
maximum E_x , V/m	4000
maximum J_y , A/m ²	13,375
maximum Hall parameter	7.3
diffuser pressure recovery	0.85
d-c power output, MW _e	848
enthalpy extraction ratio,%	35.9

^aSegmented Faraday (Fig. 5) MHD generator configuration. The fuel is Illinois No. 6 coal.

^bHHV = higher heating value.

^cTo convert MPa to psi, multiply by 145.

^dTThe loading parameter varies along the channel.

5.1. Plant Economics

A power plant is evaluated economically in terms of capital costs (\$/kW) and levelized costs of electricity (mills/kWh = 10^{-3} /kWh). Important factors are the escalation of costs with time and the cost over time of the capital to build the plant. Table 5 gives the distribution of plant capital costs in percent of plant direct costs, and shows the relative cost of components and subsystems specific to the MHD topping cycle for two first generation commercial MHD power plants of 200 and 500 MW output. The most costly item is the steam generator with oxidant preheater. The second most costly item is the superconducting magnet, which costs slightly more than the oxygen plant. A more recent estimate of capital costs gives a range of \$1300 – 1320/kW for a 600 MW plant (66). Figure 12 shows the variation in plant capital costs with plant size (44). Costs are normalized with respect to the modified reference steam plant of 800 MW nominal capacity used in the Energy Conversion Alternatives Study (ECAS) (41, 42) and are based on the first generation MHD plant costs (44). Comparative estimated costs for conventional steam power plants over the same size range are also shown. The estimated capital costs (Fig. 12a) of first generation MHD power plants are somewhat higher than the capital costs of conventional coal-fired steam plants of comparable output, for the range of plant sizes studied. Calculated levelized costs of electricity shown in Figure 12b are lower for the MHD power plants than for comparably sized conventional steam power plants, by about 7.4% for the 950 MW plant, 7.1% for the 500 MW plant and 3.3% for the 200 MW plant. Not surprisingly, the savings become less as the plant becomes smaller. The costs in Figure 12b are based on the capital cost curve (Fig. 12a) and fuel costs based on the modified ECAS reference steam plant efficiency of 34.3%. The cost comparisons are based on a coal price of \$1.00/GJ

Table 5. Cost Distribution for MHD–Steam Base Load Power Plants^{a, b}

Parameter	Cost, ^c %	
	500 MW Plant	200 MW Plant
land,%	0.25	0.37
structures and improvements	9.54	11.77
boiler plant		
coal and ash handling	5.36	5.05
steam generator with oxidant heater	21.61	20.41
effluent control and other	4.50	4.42
steam turbine generator	9.24	10.35
accessory electric equipment	6.17	6.00
miscellaneous power plant equipment	0.47	0.63
MHD topping cycle		
combustion equipment	6.0	6.14
MHD generator	1.59	1.23
magnet subsystem	9.84	10.89
inverters	8.09	6.94
oxidizer supply subsystem	1.98	1.74
oxygen plant	9.20	7.83
seed subsystem	4.87	4.88
transmission plant	1.29	1.34
subtotal direct costs	100.00	100.00
engineering services and other costs	10.00	10.00
overnight construction costs	110.00	110.00
interest and escalation	9.00	8.00
total construction cost with IDC and EDC ^d	119.00	118.00
specific plant cost ^e with IDC and EDC, ^d \$/kW	838	1090

^aRef. 44^bFuel costs are taken to be \$1.00/GJ (\$1.05/MBtu); the escalation and interest rates are 6.5% and 10%, respectively; and the factor used for calculating levelized fuel and operating and maintenance cost is 2.004.^cConstruction time period is assumed to be 4.83 years and 4.33 years for the 500 and 200 MW plants, respectively.^dIDC = interest during construction; EDC = escalation during construction.^eIn mid-1978 dollars

(\$1.05/MBtu). Higher fuel costs would increase the attractiveness of MHD because of its more efficient use of the fuel.

6. Components and Subsystems

6.1. High Temperature Air Preheaters

Combustion air–oxidant preheating for open cycle generators is accomplished in one of two ways. One way is to use the heat energy of the MHD generator exhaust gas directly; in this case, the preheater is classified as directly fired and is located in the MHD generator exhaust as part of the bottoming plant (Fig. 3). The other way of preheating combustion air is to use a separate heat source using clean fuel. This type of preheater is classified as separately fired. Directly fired preheat offers the potential of higher cycle efficiencies than can be achieved with separately fired preheat, at the same oxidizer temperature. However, because of the severe difficulties associated with designing a directly fired preheater capable of operating with the seed and ash-laden gases flowing from the generator, first-generation commercial plants are to use separately fired preheat.

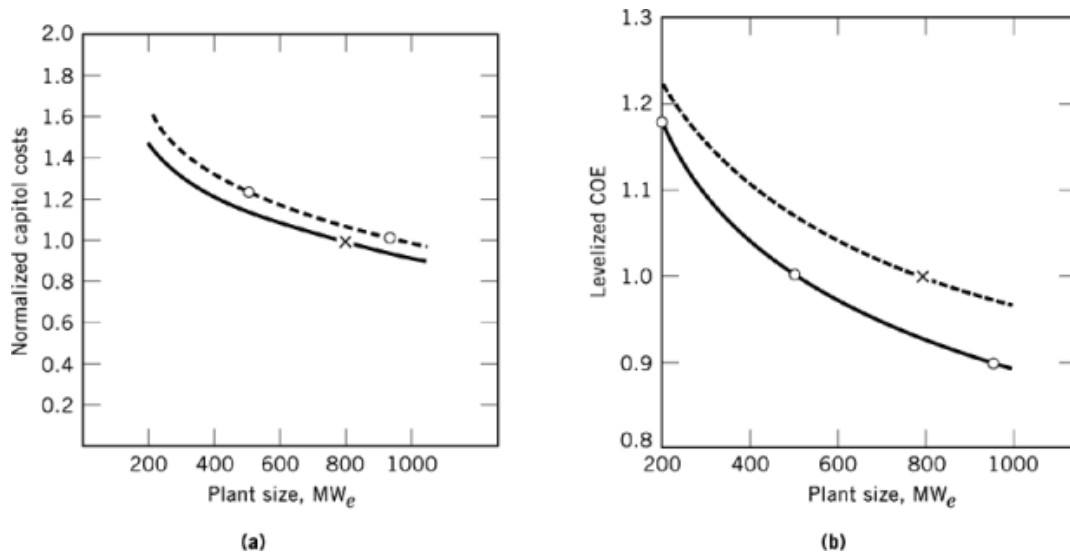


Fig. 12. Costs as a function of plant size for (—) coal-fired steam plants and (---) early MHD power plants where \times corresponds to the ECAS reference plant costs. (a) Normalized capital (IDC and EDC are not included) and (b) levelized cost of electricity (normalized) where IDC and EDC are included and the LEV factor is 2.004 (44) (see Table 5).

Air preheat temperature requirements of 2250–2300 K are anticipated for natural gas-fired systems, and about 2000 K for oil or coal-fired systems (11). Use of 32–40% oxygen enrichment lowers the preheat temperature requirement to a moderate 900–1000 K, which can be attained with conventional metal-type tubular heat exchangers. Depending on the cost of oxygen, this is a viable alternative to the use of separately fired high temperature preheaters.

More advanced MHD power plants of the future are expected to use preheat temperatures of up to 2000 K. These temperatures, to be achieved by direct firing, require the use of high temperature regenerative heat exchangers, where heat is transferred for a time from a hot fluid, eg, the MHD generator exhaust gas, to a medium which subsequently transfers the heat to a cool fluid, eg, the incoming combustion air. While heat is transferred to the incoming air, the MHD exhaust is directed to a second regenerative preheater operating identically. The two preheaters operate cyclically to provide continuous heating of the combustion air. The other type of heat exchanger is the recuperator, in which heat is transferred continuously from one fluid to another through a solid wall which separates the two fluids. Metallic recuperators are used widely in industry, but are limited for MHD use to about 1250 K, because of corrosive problems caused by seed and ash, as well as mechanical strength problems caused by the pressure requirements. Whereas ceramic recuperators can operate at higher temperatures, development of ceramic recuperators for MHD has not been pursued because of severe problems related to fabrication, fluid leakage, and mechanical strength.

Regenerative heat exchangers of both the fixed-bed and moving-bed types (67) have been considered for MHD use. The more recent efforts have focused on the fixed-bed type (68), which operates intermittently through recycling. A complete preheater subsystem for a plant requires several regenerators with switch-over valves to deliver a continuous supply of preheated air. The outlet temperature of the air then varies between a maximum and a minimum value during the preheat cycle.

Fixed-bed regenerators have been used in the glass (qv) and steel (qv) industries to preheat air to 1350–1650 K, but these operate with relatively clean gases compared to the MHD combustion gases. One design, fabrication and testing of a regenerator for MHD use, involved a regenerator matrix, or bed packing, of 8.5

m in height and 7.9 m in dia (68). The matrix geometry consisted of cored bricks, or checkers, made of fusion cast magnesia–spinel. Cycle times were 1280 seconds on MHD gas flow, 760 seconds on oxidant flow, with 360 seconds for switching. Operating times up to 1470 hours were achieved. System heat, leakage (oxidant mass loss to the MHD heating gas and MHD gas loss to the oxidant), and pressure losses were all within acceptable limits. High temperature refractory-lined water-cooled gate valves were also developed and tested for up to 1390 hours and 2100 cycles at temperatures of 1860–1925 K and inlet pressures to 800 kPa (8 atm).

For gas-fired systems the state-of-the-art is represented by the preheater described in Reference 69. A pebble bed instead of a cored brick matrix is used. The pebbles are made of alumina spheres, 20 mm in diameter. Heat-transfer coefficients 3–4 times greater than for checkerwork matrices are achieved. A prototype device 400 m³ in volume has been operated for three years at an industrial blast furnace, achieving preheat temperatures of 1670 to 1770 K.

6.2. Combustor

In the majority of MHD plant designs the MHD combustor burns coal directly. Because MHD power generation is able to utilize pulverized coal in an environmentally acceptable fashion, there is usually no need to make cleaner fuels from coal, eg, by gasification or by beneficiation. A discussion of combustion techniques for MHD plants is available (70).

The function of the MHD combustor is to process fuel, ie, coal; oxidizer, ie, preheated air, possibly enriched with oxygen; and seed to generate the high temperature electrically conducting working fluid required for the MHD channel. There are several design requirements: (1) highly efficient combustion, ie, high carbon conversion and low heat losses, in order to achieve the temperature (2800–3000 K) required for adequate electrical conductivity; (2) innovative wall designs capable of extended life, to contain 500–1000 kPa (5–10 atm) of pressure in the presence of molten slag, seed, and heat fluxes up to 50 W/cm²; (3) spatially and temporally homogeneous output flow, requiring sophisticated aerothermodynamic design; (4) low pressure drop through the combustor, because this directly affects the net power output of the MHD topping cycle; (5) effective seed utilization, which means minimizing slag–seed interactions which remove seed from the gas, and attaining uniform seed dispersion; (6) electrical isolation of the combustor and its ancillary systems at voltages of 20–40 kV below ground potential, because of the electrical contact of the combustor with the MHD channel (this is particularly challenging for the slag-rejection system); and (7) efficient slag rejection, up to ~ 50 – 70% of the ash content of the coal burned, as low slag rejection (high ash carry-over) increases seed recovery costs. These design requirements differ sufficiently from those of conventional coal combustors so as to require essentially new technology for the development of MHD coal combustors.

A process receiving considerable attention as a way of burning coal and rejecting ash as slag is that used in the cyclone furnace (71). Vortex flow in the chamber promotes efficient combustion, by maintaining continuous ignition. Strong radial accelerations promote separation of particles and slag droplets and tend to bring the unreacted oxidant (cool air) into contact with coal particles on the chamber wall. The wall is protected primarily by a layer of molten slag, which also reduces the heat flux. There would normally be considerable ash vaporization in a high temperature vortex coal combustor but this can be minimized by use of a two-stage configuration. The idea of the two-stage cyclone coal combustor for MHD systems was first introduced in 1963–1965 (72).

Combustors based on this concept have been built and operated by TRW, Inc. (73, 74). A diagram of a 250 MW_t combustor design is shown in Figure 13. A precombustor stage is used to supply 1867 K to the first stage, which is a confined vortex flow chamber. The first stage is connected to the second stage via a deswirl section (not specifically identified in the figure), designed to provide uniform flow to the second stage. The second stage connects the combustor to the MHD channel.

The first stage is the slagging stage, in which slag separation and tap-off occur. Coal, having particle size distribution of 70% through 200 mesh (74 μ m), is injected at the head end via multiple injection ports.

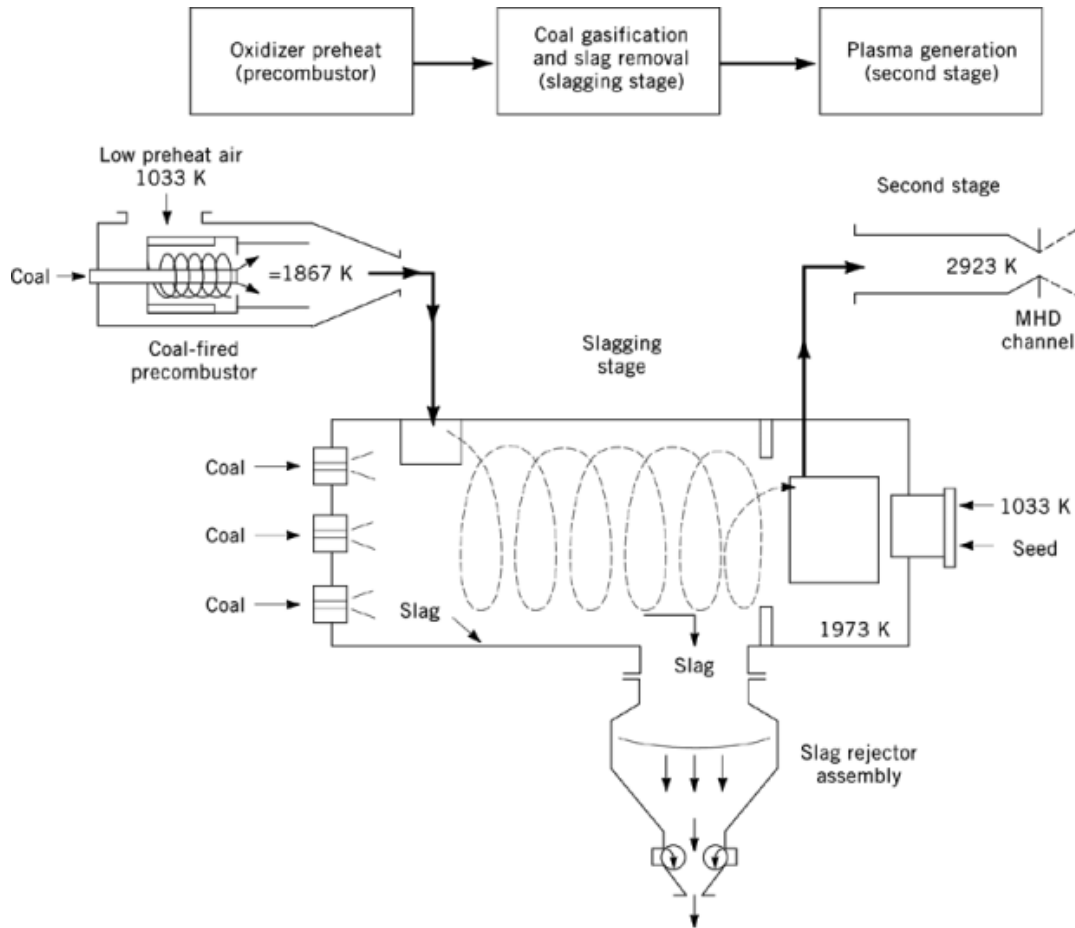


Fig. 13. Schematic of 250 MW_t coal-fired combustor.

Combustion of the coal particles is designed to occur in flight. The first stage operates essentially as a gasifier, and has an oxidizer/fuel ratio of about 0.6. The balance of the oxidizer is admitted to the deswirl section, immediately before the second stage, to bring the final stoichiometric ratio up to 0.85. Because the slag is tapped off in the first stage, the fuel supplied to the second stage is largely ash-free. Hence, seed is also injected in the deswirl section, as the relative absence of slag here means that the removal of seed from the gas by means of slag–seed reactions is minimized.

The combustor is designed to operate at a pressure of 600 kPa (6 atm) with 1867 K preheated air. First stage heat loss of the 250 MW_t combustor is about 4.3% and the total heat loss is about 6%. The relative pressure drop is 3%. More complete discussions of the design and scale-up of the combustor are available (75).

The combustor is assembled of flanged, spool-shaped water-cooled metal components, each with its own water-cooling circuit and pressure shell. No ceramic linings are used. Gas pressure is contained by stainless steel outer shells and the internal surfaces subject to high heat fluxes are lined with low alloy water-cooled panels.

Other approaches to slag-rejecting coal combustors have been taken by Rocketdyne (76) and Avco (77), which have built and operated units at the 20 MW_t scale. The Rockwell design is a two-stage device where

32 MAGNETOHYDRODYNAMICS

two first stage combustors fire tangentially into a ceramic-lined cyclone slag separator, and are followed by a water-cooled second stage. The Avco approach utilizes a single-stage cylindrical configuration with downward combustion flow, horizontal exit flow, and slag separation by means of toroidal vortices at the dome at the top of the cylinder. Descriptions of other slag-rejecting combustors are available (78–81) as is that of a system employing a combustor from which 100% of the slag passes downstream to the MHD generator (82).

The principal combustor ancillary systems are the systems for coal feed, slag rejection, water cooling, and high temperature oxidant supply. All are required to be electrically isolated from ground. Of particular interest are the first two systems. The coal feed systems required to feed the coal into the pressurized combustion chambers utilize dense phase coal transport having solids to gas mass ratios up to 200:1. These are in contrast to the more common dilute phase or slurry transports commonly used in industrial systems. Electrical and pressure isolation are achieved by use of batch mode material transfer from consecutive hoppers, separated from each other by air gaps. The slag rejection system operates in the same fashion and has the additional requirement that the slag must be kept from freezing solid and blocking flow passages. A detailed modeling of dense phase coal transport may be found in Reference 83. Systems in use are described elsewhere (84–87) as is a slag rejection system (88).

6.3. MHD Channel

The MHD channel, the heart of the MHD power generation system, is the component which produces the MHD power. Channel requirements determine the principal specifications for other components and subsystems of the MHD power plant. The basic requirements for channel development are governed by overall plant requirements of high plant reliability and availability, high coal-pile to bus-bar efficiency, and low cost of electricity. To satisfy these plant requirements, three primary MHD channel design criteria can be identified (11, 44): (1) duration or operating time between maintenance periods; (2) fraction of thermal energy input extracted from the gas as electric power output (enthalpy extraction ratio); and (3) isentropic efficiency, the ratio of the actual enthalpy change of the gas flowing through the channel to the enthalpy change of an isentropic flow at the same pressure ratio. The isentropic efficiency is closely related to the local electrical efficiency defined in equation 8, but is somewhat lower for the typical Mach numbers of interest, in the range 1–2. For early commercial plants, the channel goals are operational for several thousand hours between scheduled maintenance, and enthalpy extraction of at least 15% at isentropic efficiency of 60% or greater.

6.3.1. Construction

From a construction and fabrication point of view, the channel must provide a secure means of containing the working fluid from the combustor and a means of conducting current from the working fluid to the external load, and have adequate durability to satisfy overall power system requirements. Issues related to durability have dominated the development of channel construction methods, particularly of those surfaces which face the hot conducting gas. These surfaces consist of electrodes, which are the current-carrying elements, and insulators, which separate the electrode walls. Durability issues and the resulting designs of gas-side surfaces for coal-fired channels differ from those for clean fuel-fired channels. Channel operating on clean fuels, eg, natural gas, can use a variety of high temperature ceramic materials for both electrode and insulator surfaces which cannot be used in coal-fired channels, because of the incompatibility with molten slag. This allows operation with hotter walls and reduced electrical and thermal losses compared to coal-fired channels. The latter are typically built using cooled metal walls better able to survive the environment. Natural gas-fired channels have been studied extensively (89). The emphasis, however, has shifted to coal-fired MHD systems, both in the United States and elsewhere.

6.3.2. Durability

Two lifetime-limiting mechanisms have been identified from long duration channel tests using slagging flows (90): (1) electrochemical erosion of channel gas-side surfaces, which occurs over relatively long durations at nominal channel operating conditions; and (2) localized electrical or thermal faults, which can cause serious damage to the channel walls. The mechanisms affecting channel gas-side erosion differ for anode, cathode, and insulator walls. Anodes are subject to electrochemically induced oxidation and/or attack by sulfur (91). The erosion is caused either by oxygen or sulfur which is driven to the anode surface by the electric field, or which is chemically bound in the slag and released by arc current transport through the slag layer.

Cathode and insulator walls are less subject to severe electrochemical attack. In the case of the cathode wall, this is because of the reducing conditions which prevail, and in the case of the insulator wall, because the wall nominally carries no current. However, certain surfaces of cathode and insulator walls are anodic with respect to other surfaces, because of the axial electric field present in the generator, and these surfaces do require protection against electrochemical attack.

Besides gas-side surface erosion, the other important life-limiting mechanism is damage caused by interelectrode faults. These manifest themselves in two ways. The first, axial leakage current between adjacent electrodes, from electrically positive to electrically negative surfaces, results in gradual electrolytic corrosion of the anodic (positive) surface. The second, and perhaps more serious, fault mechanism is arcing between adjacent electrodes, which results from complete breakdown of the interelectrode gap (92, 93). This sharply increases the erosion of the corners of the affected electrodes and results in rapid destruction of the interelectrode insulator. Interelectrode arcs are particularly dangerous on anode walls, where they are driven by the Lorentz force into the wall structure and can cause severe damage.

The effects of interelectrode arcs are minimized, first, by limiting the power which can couple into such faults and second, by designing wall structures which can withstand the effects of the arcs.

For a given channel power density the fault power in the channel is proportional to the square of the electrode pitch, ie, the distance between the centers of adjacent electrodes, times the electrode length in the magnetic field direction (94). Hence, the most effective way to limit fault power in the channel is to minimize the electrode pitch. About 2 cm is the practical minimum value in large channels, limited by manufacturing constraints. Once the minimum electrode pitch has been established, fault power can be limited only by limiting the length of the electrode parallel to the magnetic field, ie, by transverse segmentation of the electrodes. In all cases the electrode current must be controlled to avoid large current overloads which can greatly increase the available fault power. Acceptable values of fault power are of the order of a few hundred watts for existing channel designs.

On a slag-covered cathode wall, leakage currents flow through the slag layer. This has the effect of electrically short-circuiting individual cathodes, typically in groups of 3–5, so that each shorted group acts like a single cathode (95). The accumulated Hall voltage, which would normally be divided approximately equally over each interelectrode gap, then appears across only one gap, that is, between one shorted group of cathodes and its downstream neighboring group. Such a pattern can be seen in Figure 14 for a Faraday-loaded generator, which shows clearly the effects of the slag layer on the cathode wall, and the contrast between anode and cathode walls. The large nonuniformities on the cathode walls are caused by the presence of electrically conducting slag constituents, such as potassium compounds or iron and iron oxide compounds, which are driven to the cathode wall by the electrical field in the channel (96). Cathode wall nonuniformities are not as harmful as anode wall nonuniformities. Locally, however, the insulator walls experience high electrical stresses. Also, in uncontrolled diagonal operation, cathode wall nonuniformities are reflected on to the anode wall through the diagonal cross-connection, accompanied by possible increase in anode interelectrode current leakage and the associated harmful effects. Current controls on the cross-connections are used to prevent this from occurring.

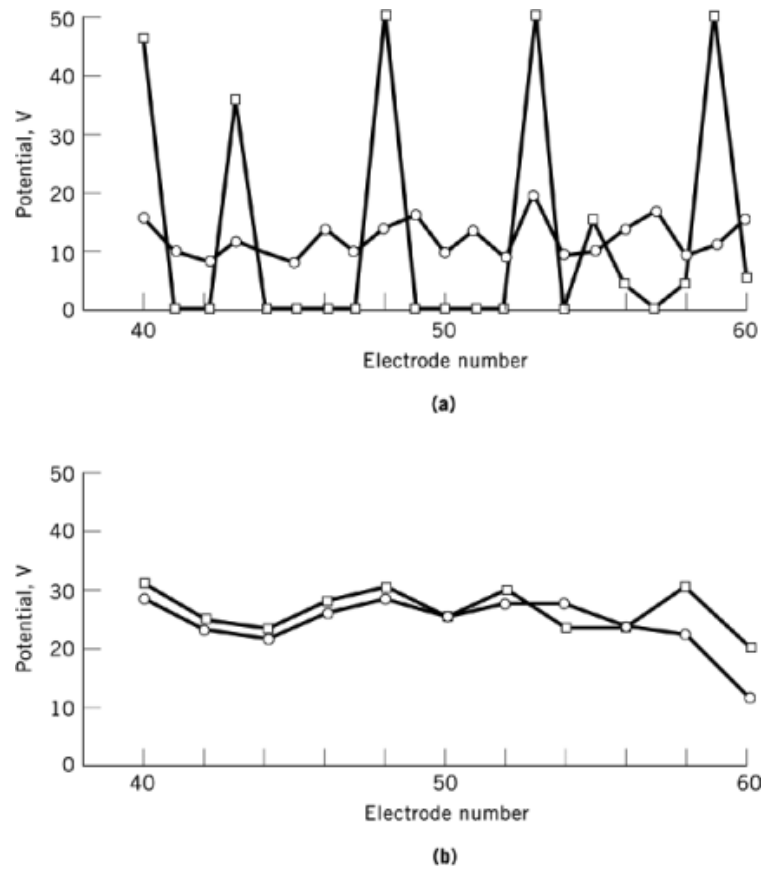


Fig. 14. Effects of slag on interelectrode walls for (□) slagged and (○) unslagged systems for (a) cathode and (b) anode interelectrode voltage.

6.3.3. Gas-Side Surface Design

6.3.3.1. Electrode Walls. Development of durable electrode walls, one of the most critical issues for MHD generators, has proceeded in two basic directions: ceramic electrodes operating at very high surface temperatures (≥ 2000 K) for use in channels operating with clean fuels such as natural gas, and cooled metal electrodes with surface temperatures in the range 500–800 K for channels operating with slag or ash-laden flows.

The hot ceramic electrodes tend to operate with diffuse transport of current from the plasma to the electrode surface, reduced tendency for interelectrode breakdown, and reduced heat losses. The most common designs, developed for the U.S.S.R. High Temperature Institute gas-fired U-25 channel, use zirconia electrodes either brazed to metal substrates made of special stainless steel or chromium alloys, or else rammed on to metal substrates reinforced with wire mesh (97, 98). The zirconia is doped with rare-earth oxides such as yttria or ceria; other oxides such as calcia have also been used, particularly in the formulations designed for ramming. Typical compositions are $0.88 \text{ ZrO}_2 + 0.12 \text{ Y}_2\text{O}_3$, or, for the calcia-stabilized ceramics, $\text{Zr}_{0.85}\text{Ca}_{0.15}\text{O}_{0.15}$ (99). Electrical current in these ceramics is transported primarily by oxygen anions. Another class of ceramic electrodes is based on materials such as lanthanum chromite (100) or silicon carbide; in these materials current transport is electronic rather than ionic, and electrical conductivity is higher. Also, thermal conductivity is

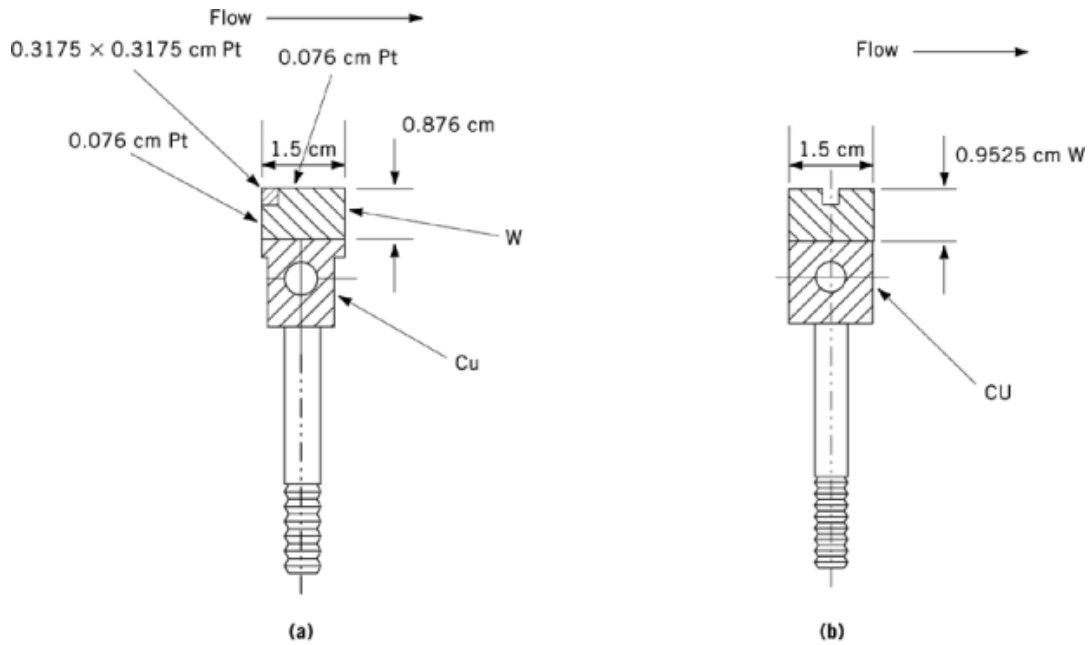


Fig. 15. Designs of an MHD (a) anode and (b) cathode.

higher than in zirconia-based ceramics. A disadvantage is that their maximum operating temperatures are lower, in the range 1400–1600 K, compared to the 2000–2200 K capability of zirconia.

Although ceramic electrodes have received much attention (101), they have not been successful in channels operating with slag-laden flows, because of excessive electrochemical corrosion caused by the slag. Only well-cooled metallic elements have been used successfully in slagging environments.

An important feature of slag-covered metal electrodes is that current transport to both electrode walls, anode and cathode, is via arcs (95). Hence, a well-cooled structure having good thermal diffusivity is required. Water-cooled copper has been used successfully for many years in developmental channels. Metal electrode walls are designed to retain a slag coating so that a higher gas-side surface temperature (ca 1700 K) can be maintained than is possible for bare metal walls. This reduces electrode voltage drops and heat losses.

The main cause of anode wear is electrochemical oxidation or sulfur attack of anodic surfaces. As copper is not sufficiently resistant to this type of attack, thin caps of oxidation and sulfur-resistant material, such as platinum, are brazed to the surface, as shown in Figure 15a. The thick platinum reinforcement at the upstream corner protects against excessive erosion where Hall effect-induced current concentrations occur, and the interelectrode cap protects the upstream edge from anodic corrosion caused by interelectrode current leakage. The tungsten underlayer protects the copper substrate in case the platinum cladding fails.

Other cap materials have been tested, but in regions of the channel where the electrical and thermal stresses are the highest, the most successful, ie, longest lifetime, electrode design has platinum caps operated at low (ca 500 K) temperatures. Anodes of like design, but without the tungsten back-up layer, have been operated successfully for more than 1000 hours in a slag and sulfur-laden flow (102), at electrical and thermal stresses similar to those expected in commercial-sized generators.

Cathodes are less subject to erosion by electrochemical attack than are anodes because reacting ionic species are not released in the cathode slag layer. A viable cathode design (Fig. 15b) is a cooled copper substrate capped with tungsten—copper to resist microarcs and mechanical erosion by slag. An earlier design incorporated

a cap of TD nickel on the upstream side, which is an anodic surface with respect to the neighboring upstream cathode. This design was operated successfully for 500 hours (103) and the erosion rates were low enough to indicate that much longer lifetimes can be expected. A modified version was operated for 250 hours, with even lower erosion rates.

The interelectrode insulators, an integral part of the electrode wall structure, are required to stand off interelectrode voltages and resist attack by slag. Well cooled, by contact with neighboring copper electrodes, thin insulators have proven to be very effective, particularly those made of alumina or boron nitride. Alumina is cheaper and also provides good anchoring points for the slag layer. Boron nitride has superior thermal conductivity and thermal shock resistance.

6.3.3.2. Insulator Walls. Because of the unavailability of electrically insulating materials which can withstand the harsh environment inside coal-fired channels, the insulator walls of the channel are typically made of metal elements which are insulated from each other to prevent any net flow of current. Like electrode walls, insulator walls are designed to operate with a slag coating.

Figure 16a shows a so-called peg wall design, in which thin insulators separate rectangular or square metallic elements, ie, pegs, typically 2–3 cm on a side. The advantage of the design is its superior electrical insulating properties under all operating conditions, and its electrical flexibility. The disadvantage is the mechanical complexity arising from the large number of small elements. However, using proper engineering and assembly procedures such walls can be made to operate reliably and have, in fact, been tested at 20 MW_{th} scale for hundreds of hours (103).

To simplify insulator wall design, the continuously conducting sidewall, shown in Figure 16b, is used. The elements lie nominally along equipotential lines in the generator. This type of construction does not allow external current control or fault power control. Also, although the sidewall elements lie nominally along equipotential lines, exact alignment is not possible, as the equipotential lines are not straight, owing to boundary layer effects and load variation. The sidewalls in fact do collect some current which tends to concentrate near the channel corners, causing erosion at these locations (104).

To alleviate these problems, the continuous side bar is split, as shown in Figure 16c. Each sidewall segment is large enough to be individually water-cooled. In comparison to the single side bar design, the segmented bar requires a larger number of water hoses and penetrations of the pressure vessel, but far fewer than the peg wall design.

6.3.4. Mechanical and Thermal Design

The main objectives of channel mechanical and thermal design are to maintain structural and sealing integrity, to provide adequate cooling of gas-side surface elements, and to use efficiently the magnet bore volume, ie, to maximize the ratio of channel flow cross-section area to the magnet bore cross-section area. This last requirement affects not only the channel mechanical design but also the packaging of channel electrical wires, cooling hoses, and manifolds. In broad terms, MHD channels built to date have fallen into one of three types of construction categories: plastic box construction; window frame construction; or reinforced window frame construction.

In plastic box construction an example of which is shown in Figure 17, the channel is a four-wall assembly. Each wall consists of the individual gas-side surface elements mounted on an electrically insulating board, which is made typically of a fiber glass-reinforced material such as NEMA Grade G-11. The box formed by assembly of the four walls serves as the main structural member and the pressure vessel of the channel. Final gas-side contouring is done by varying the height of the electrodes and insulating wall elements. Gas sealing is done on the edges of the plastic wall, along the corners of the box. The Textron 1A4 channel (Fig. 17) (104) has operated for hundreds of hours. Other channels built in this manner include the Mark VI and Mark VII channels built by Avco (105) and the high performance demonstration experiment (HPDE) channel (106). The most extensive data base has been accumulated for this type of construction.

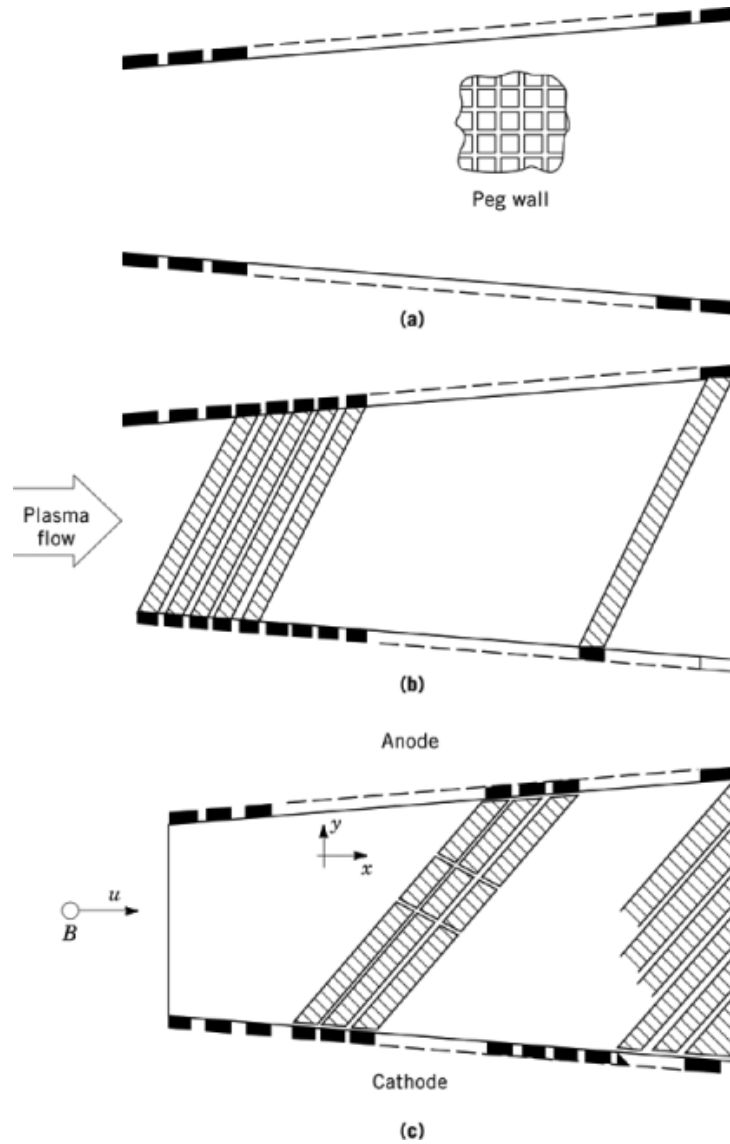


Fig. 16. Insulator wall designs: (a) peg wall; (b) conducting bar wall; and (c) segmented bar wall. The gas-side materials are tungsten and tungsten–copper composite, the base material, copper, and the insulators, boron nitride. Slagging grooves are shown.

Plastic box construction has several advantages: it is readily scalable to large commercial sizes; readily separable walls make assembly, disassembly, and refurbishing of the walls relatively simple, fast, and inexpensive; noncurrent carrying sidewalls can be used, which permits the use of local current controls; gas sealing and interelectrode insulator functions are separated, thus minimizing the risk of plasma leakage in the event of interelectrode breakdown and arcing; and there are only four main gas seals, along the corners of the box, further minimizing the risk of plasma leakage. The main disadvantage is the large number of cooled elements

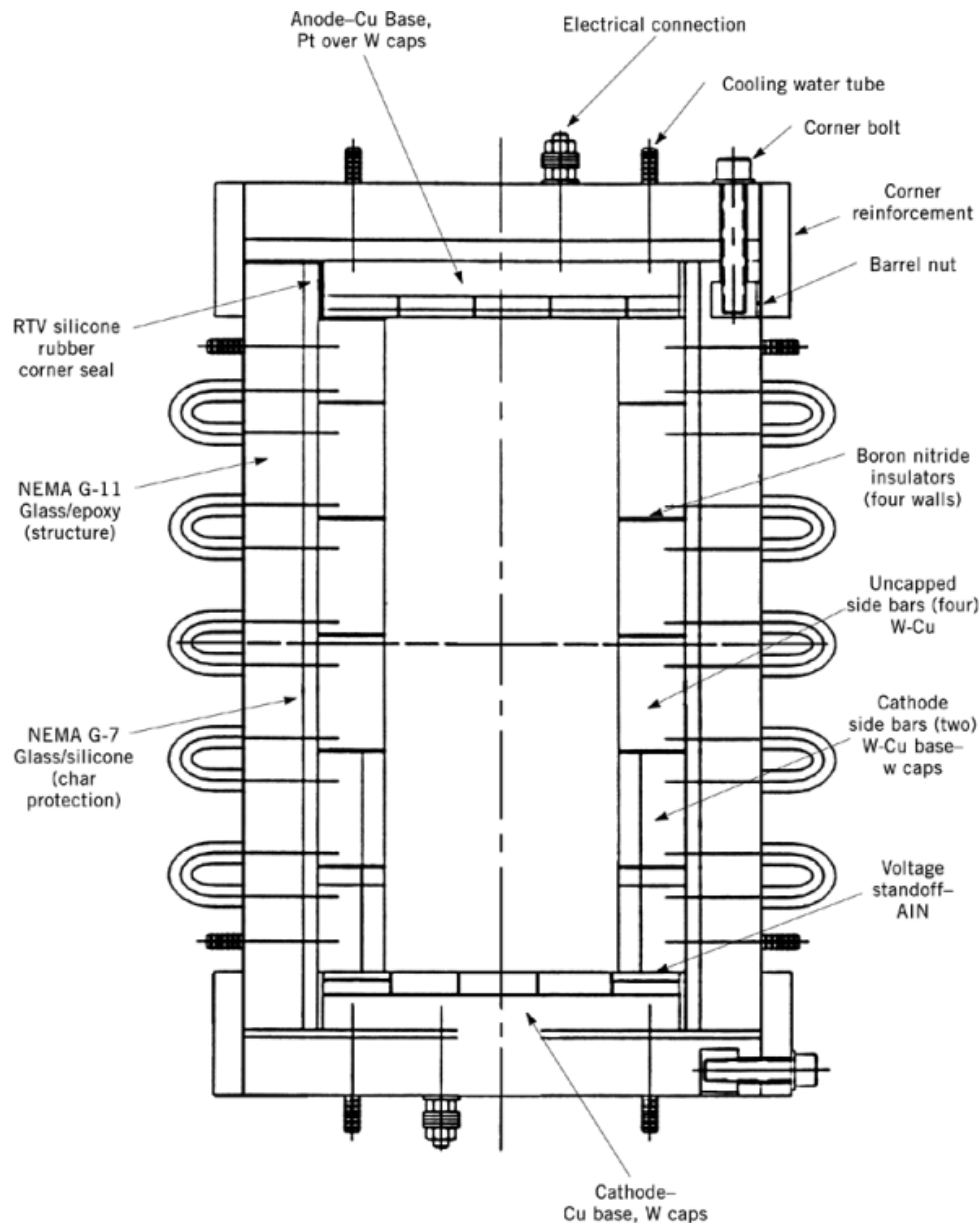


Fig. 17. Schematic of plastic box Textron 1A4 channel (104).

that either carry current or must be electrically insulated from each other, and the associated large number of water hoses and electrical wires that are required.

The window frame channel design (Fig. 18) is made by stacking together metallic frames inclined at the same angle as the generator equipotentials. The frames serve as both the current-carrying elements and as the pressure vessel of the channel. Gas sealing is done around the perimeter of each frame, at some distance

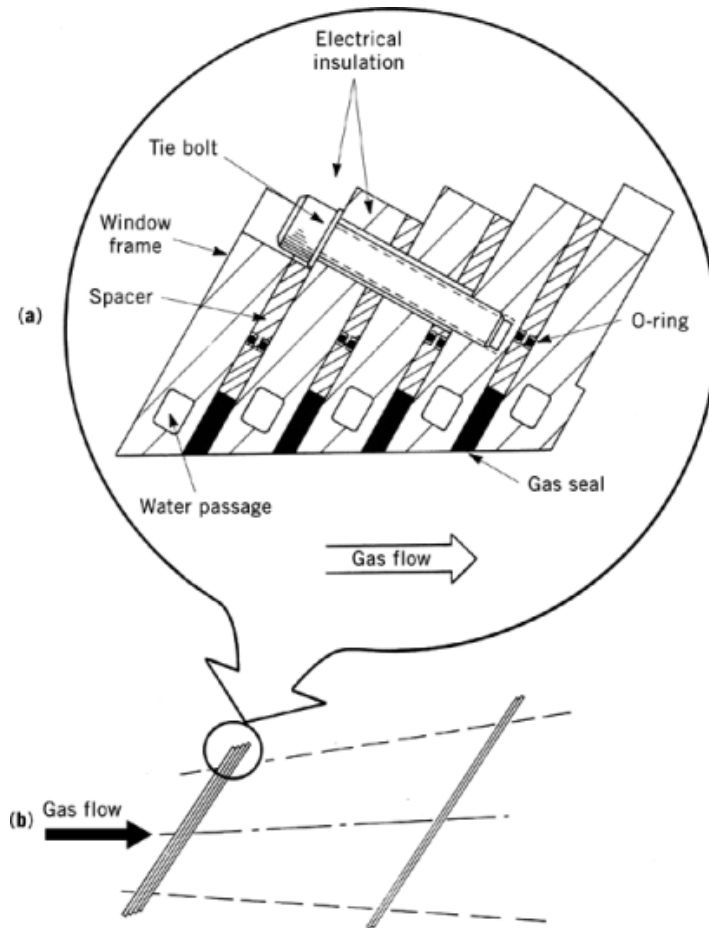


Fig. 18. (a) Window frame channel construction, and (b) extended view of channel.

from the gas. Window frame construction was used for the Lorho generator (107), a large Hall generator built by Avco, and for another large channel built in the United States for use in the Russian U-25 facility (108).

Window frame channels offer several advantages: the continuous metal frames have good strength and can be assembled to form a rugged structure; electrical simplicity is achieved by using the frames as the current carrying elements, thus minimizing the amount of external wiring for this purpose; and hydraulic reliability is maximized by reducing the number of hydraulic circuits.

Offsetting these advantages are some serious disadvantages. First, the great length of sealing surface (equal to the frame perimeter times the number of frames), together with the fact that gas sealing and structural functions are combined, make this type of construction vulnerable to hot gas leaks. Second, scaling to commercial sizes is difficult because of the problems associated with fabrication of large window frame channels. A pilot-plant size channel may have about 500 frames, each about 2-cm thick and about 1-m long on a side, requiring great care to avoid bending and distortion during handling. Also, water passages are difficult to incorporate into such frames. Third, a commercial-scale window frame channel of minimum practical pitch, at conditions typical of full-scale operation, has a very high fault power because of the large continuous length of frame, and offers no possibility of fault power control either by segmentation or by frame current control.

The reinforced window frame channel, eg, the large Russian RM channel (109) and the smaller Russian U25B channel (110), is essentially a window frame channel inside a plastic box which serves as the pressure vessel and main structural member. It combines some features of both window frame and plastic box construction. Frames can be segmented, although with some difficulty, for fault power control. This construction is difficult to disassemble for inspection and/or refurbishment.

Channel thermal design, although requiring care, poses no significant problems. Heat fluxes from the gas to the walls of the channel can range from 50 W/cm^2 at the exit of a well slagged channel to about 500 W/cm^2 at the inlet of an unslagged channel. Coolant flow velocities in gas-side surface elements are typically in the range $2 - 5 \text{ m/s}$. Coolant hoses, manifolds, etc, must have adequate mechanical and thermal properties, and also be electrically insulating, in order to avoid electrical shorting of channel elements. These requirements limit the types of hoses and manifolds which can be used, and therefore the allowable cooling water pressure and temperature.

The operating durations achieved by various combustion-driven experimental channels is shown in Figure 19. The electrochemical and thermal stress levels of an Avco Mk VI channel, operated for 500 h, (103) were similar to those expected in commercial coal-burning plants. Results indicate that durability of properly designed and operated channels can be extrapolated to several thousand hours. This test conducted in two over 300 hour segments was performed prior to the availability of adequate MHD coal combustors. Coal-burning operating conditions were simulated by injecting ash and sulfur into an oil-fired MHD combustor. Another significant demonstration used actual coal-fired operation at the CDIF for over 300 hours. The generator was operated at power outputs up to 1.5 MW_e .

Figure 20 shows values of the channel enthalpy extraction ratio for a number of channels. Enthalpy extraction (111) equal to that required by a proposed demonstration plant (112) has been achieved. Channels have performed generally in accordance with predictions.

Whereas considerable progress has been made towards achieving acceptable channel performance (power and enthalpy extraction) and durability, as of this writing performance and durability have not been demonstrated simultaneously. A larger scale demonstration plant has been proposed in the United States by the MHD Development Corp. (112).

Further work is also required in the area of mechanical design and construction of large MHD channels, especially with respect to construction features which are scalable to commercial size channels. The mechanical design of channels is aimed first, at achieving electrical and structural integrity of the channel, and second, at achieving the most efficient use of the magnet bore in order to minimize the required volume of magnetic field, and hence, the magnet cost. This is done by compact packaging of channel structure, electrical wiring, water manifolds, hoses, etc. Additional important considerations are channel installation, maintenance, and repair.

6.4. Electrical Loading and Control

The function of the channel loading system is to extract from the channel the power generated in each plasma element with minimal losses (113, 114). This means that the load circuit impedance must match as closely as possible the channel impedance at all axial locations along the channel, which is achieved by use of multiple power take-off points. Ultimately, power from the separate take-offs must be consolidated into a single terminal pair at the transmission grid, by means of appropriate circuitry. An inverter is necessary between the channel and the transmission grid in order to convert the relatively low voltage (20–40 kV) dc output of an MHD generator to ac at transmission line voltages (200–400 kV). In principle, the power consolidation function can be combined with the inversion function by use of common circuitry; in practice, it is simpler and less costly to separate these functions.

Segmented Faraday generators and multiloaded diagonal generators require that outputs from multiple terminals at different potentials be consolidated into one set of load terminals, at the inverter. The consolidation circuitry must be nondissipative and should not change the axial voltage gradient along the channel. For the

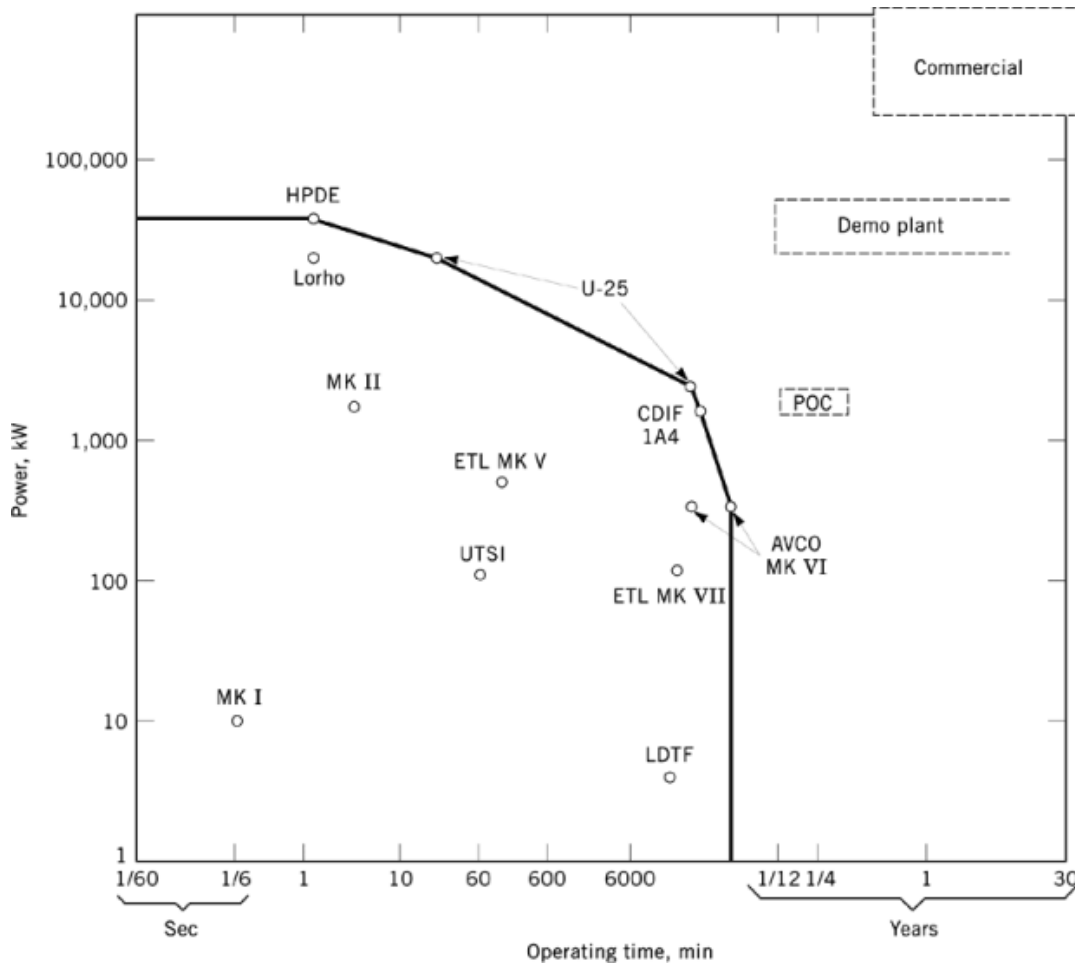


Fig. 19. Generator operating time for the various MHD facilities discussed in text: (○) achieved performance and (□) those planned. POC=proof of concept.

segmented Faraday generator, consolidation circuitry is necessary at each electrode pair, whereas for the diagonal generator this circuitry is necessary only at the power take-off regions (115). This circuitry can also be used to perform control and safety functions, such as maintaining a prescribed electrode current distribution to prevent destructive current overload of the electrodes, and to prevent nonuniformities occurring in part of the channel, eg, cathode wall, from propagating to other parts of the channel, eg, anode wall. Hence, the circuits are used at each electrode pair even in diagonal generators. The combined functions of current control and consolidation are generally referred to as power conditioning or power management. Current consolidation and control was first proposed in the 1970s (116). A number of methods for its accomplishment have been proposed (117–119). The most well-developed of these is described in detail elsewhere (119, 120). Extensive operational experience with this method, which maintains individual electrode currents at the average value of a group of electrodes, has been obtained on various channels (121).

For current consolidation, the basic circuits, used at each of the multiple power take-off points, are stacked into a Christmas tree topology to form a single power take-off terminal pair. Scale-up of these devices

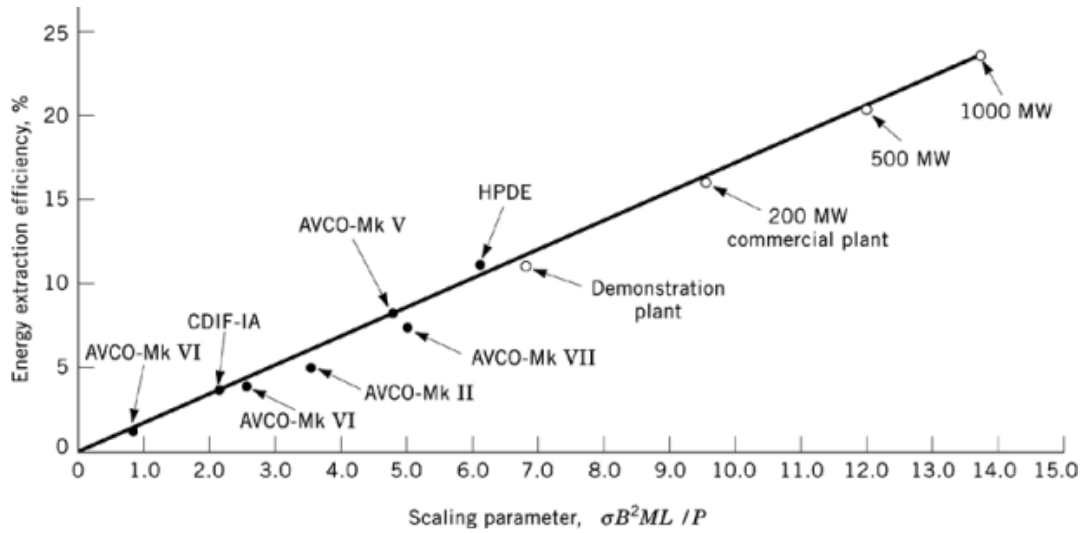


Fig. 20. Scaling of channel enthalpy extraction for the various MHD facilities discussed in text: (●) achieved, and (○) predicted where σ is the average gas conductivity in mho/m ; B , the average magnetic field in T; M , the channel Mach number; L , the average channel active length, m; and P , the average channel static pressure, kPa. To convert kPa to atm, divide by 101.3.

to commercial sizes is not expected to be a problem, as standard electrical components are available for all sizes considered. A different type of consolidation scheme developed (117), uses dc to ac converters to connect the individual electrodes to the consolidation point. The current from each electrode can be individually controlled by the converter, which can either absorb energy from or deliver energy to the path between the electrode and the consolidation point. This scheme offers the potential capability of controlling the current level of each electrode pair.

A comprehensive discussion of the design of inverters for MHD applications can be found in Reference 122. MHD inverters using both line commutation (122, 123) and forced commutation (124, 125) have been used. Line commutated systems require power factor correction and harmonic filtering, and are susceptible to loss of commutation caused by anomalous ac line disturbances. Forced commutated circuitry requires control of both real and reactive power between the inverter and the ac grid; also, its costs and losses increase with dc voltage ratio, restricting the practical voltage range. Line commutation is preferred, primarily because the technology is considered to be better developed.

6.5. Magnet

The magnetic field for utility scale MHD generators is provided by a superconducting magnet system (SCMS), for economic reasons, as the cost of electricity for a conventional magnet of the required size is prohibitive. The SCMS consists of three principal subsystems: the main magnet and cryostat subsystem, the cryogenic refrigeration system, and the power supply and protection subsystem. Of these, the magnet subsystem is the most critical, having the majority of the design choices and requiring the bulk of the engineering and manufacturing effort.

The magnet is required to provide a field of the required magnitude and, in the case of linear channels, axial profile. Linear MHD systems require a sharp magnetic field reduction at the channel ends (Fig. 21). This is to reduce the induced electric fields at the channel power take-off regions and to minimize the magnetic field

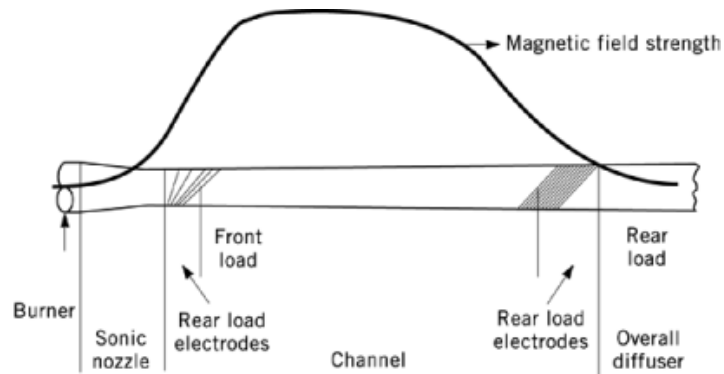


Fig. 21. Magnetic field distribution.

seen by nonpower generating components of the flow train, such as the combustor, the nozzle, and the diffuser, so as to minimize induced circulating currents which could cause erosion. Field uniformity requirements for MHD magnets are relatively modest; uniformity within $\pm 1\%$ is adequate.

The magnet is wound from a composite of niobium–titanium and copper or aluminum. The Nb–Ti is the superconductor and the copper or aluminum serves to stabilize the conductor, by providing capacity for heat absorption from the joule heating which occurs in the event that the conductor undergoes a transition from its superconducting state into a normally conducting state. Liquid helium cooling to about 4 K is necessary to maintain the superconducting state.

The composite conductor is typically wound in the form of a cable, which can be cooled either internally by a forced helium flow or externally by immersion in a pool of helium. Large electromagnetic body forces, up to 500 t/m^2 , are experienced by the conductor during operation. These are contained by a massive external structure, although designs have been proposed in which the conductor itself serves as its own force containment structure (126).

The entire magnet structural assembly must be cooled, requiring containment in a dewar with vacuum layer thermal barriers. With careful design the refrigeration power requirements can be kept to a few hundred kilowatts, even for an MHD plant producing hundreds of megawatts. Magnets of various coil geometries can be used. The solenoidal configuration, Figure 22a, is the simplest and least costly to fabricate. It is a suitable configuration for disk generators, but not for linear generators, which leave too large a fraction of the available magnetic field volume unused. In the racetrack geometry (Fig. 22b) two flat oval coils are placed opposite each other, one on either side of the channel, to provide the transverse field. This configuration is more efficient with linear channels than is the solenoidal configuration, but still wastes magnetic field volume at the ends. Another drawback of the racetrack is that it is difficult to achieve with it the required axial field profile.

The saddle-shaped configuration (Fig. 22c) is the most efficient configuration for linear channels. The two saddle shaped coils are located parallel to each other; the MHD channel is located in the gap between the two coils. The longitudinal part of the conductors lies parallel to the direction of flow in the MHD channel, the direction of the field being transverse to the flow in the horizontal plane. This configuration is the most efficient in its use of magnetic field volume and can be readily designed to provide the required axial field profile. Its principal disadvantage is that it is more complicated to fabricate.

For power plants, magnetic fields of 4.5 to 6 T ($4.5 - 6 \times 10^4 \text{ G}$) are required, over warm bore volumes having typical dimensions of 3–4 m dia and 15–20 m long. Stored energies in such magnets are 2000 MJ (480,000 kcal) or greater. The external dimensions are of the order of 15 m dia by 25 m in length. Such large structures must withstand the high mechanical loads imposed by the magnetic fields while retaining cooling

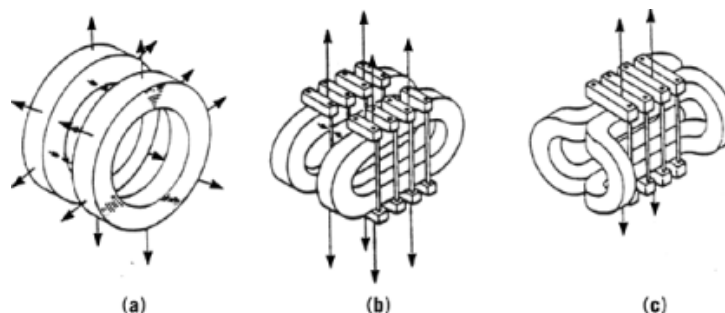


Fig. 22. Superconducting magnet configurations for MHD generators where the arrows represent the magnetic lines of force. (a) Solenoid; (b) racetrack; and (c) saddle.

integrity so that internal temperatures of 4 K can be maintained without excessive heat loss. Descriptions of a number of different design approaches can be found elsewhere (127–129).

Some technology for large superconducting magnets has been developed, mainly for bubble chamber and fusion reactor applications, and magnets having stored energy up to 500 MJ (100,000 kcal) have been built. Winding and fabrication techniques for very large saddle-shaped coils needs further development. Magnets of commercial size are too large to transport. These require field assembly with the attendant need to develop suitable fabrication techniques.

MHD superconducting magnets have been built in Japan (130, 131) and in the United States (132, 133); the largest was built in 1981 (133). This magnet, designed to be cost-effective and scalable to commercial size, was successfully operated at its design field of 6 T. Characteristics of the superconducting magnet having a horizontal peak on-axis field of 6 T and stored energy of 210 MJ (50,000 kcal) are: inlet bore diameter, 0.8 m; outlet bore diameter, 1.0 m; active field length, 3.0 m; overall height and width, $4.9 \text{ m} \times 4.1 \text{ m}$; overall length, 6.4 m; and total weight, 173 T.

Studies of MHD superconducting magnets are in progress at the Plasma Fusion Center at MIT (126, 127). These include studies of materials concerned with the properties of highly stressed structural members operating at temperatures near absolute zero, studies of superconductor configurations and winding techniques, studies of shipping and on-site assembly methods to establish the degree of modularity required, and studies of scaling factors and costs. Similar work is in progress as part of the Italian national superconducting magnet program (129) and also in India (134).

6.6. Heat Recovery and Seed Recovery System

Although much technology developed for conventional steam plants is applicable to heat recovery and seed recovery (HRSR) design, the HRSR has several differences arising from MHD-specific requirements (135, 136). First, the MHD diffuser, which has no counterpart in a conventional steam plant, is included as part of the steam generation system. The diffuser experiences high $30 - 50 \text{ W/cm}^2$ heat transfer rates. Thus, it is necessary to allow for thermal expansion of the order of 10 cm (137) in both the horizontal and vertical directions at the connection between the diffuser and the radiant furnace section of the HRSR.

Secondly, inlet conditions are more severe in the MHD HRSR because the hot gas entering the HRSR is at considerably higher temperature and enthalpy than that entering a conventional boiler. Typical radiant furnace inlet gas temperatures for the MHD plant are between 2300–2400 K, and have about 3250 kJ/kg (777 kcal/kg) enthalpy. These values are about 300 K and 500 kJ/kg (120 kcal/kg) higher than the corresponding quantities for a conventional boiler. Hence, heat transfer rates are higher in the HRSR. In addition, the gas enters the MHD HRSR with a velocity of 100 – 200 m/s, even after deceleration in the diffuser. This is higher by a factor

of 5–10 than the value encountered in conventional plants. A transition section is used between the diffuser and the furnace entrance to decelerate the gas further to prevent impingement of the particle-laden gas on the rear walls of the furnace, with the consequent risk of wall burn-out (138).

Third, design constraints are imposed by the requirement for controlled cooling rates for NO_x reduction. The 1.5–2 s residence time required increases furnace volume and surface area. The physical processes involved in NO_x control, including the kinetics of NO_x chemistry, radiative heat transfer and gas cooling rates, fluid dynamics and boundary layer effects in the boiler, and final combustion of fuel-rich MHD generator exhaust gases, must be considered.

Finally, the MHD HRSR conditions are more hazardous to the furnace materials because of the more corrosive environment (139, 140) created by the hotter combustion gases, bearing potassium, which is not found in conventional plants. Of particular concern is the effect of condensed seed compounds, mainly K_2SO_4 , on the boiler tubes and recuperative air preheater. Sulfur and ash are of course also present and detailed understanding of seed–sulfur chemistry is necessary for proper design. Research is in progress (141) to develop a detailed understanding of seed condensation, particle deposition, and fouling of heat transfer surfaces in order to develop techniques for removing slag and seed deposits from heat transfer surfaces.

Testing aimed at resolving issues of seed/ash removal and chemistry is in progress at the Coal Fired Flow Facility in Tullahoma, Tennessee, where a 28 MW_t HRSR, downstream of a coal-fired flow train, is being operated. More than 2500 hours of coal-fired testing has been performed and the measured NO_x and SO_x emissions (Figs. 9 and 10) are well below NSPS standards (53). Particulate emissions were also below NSPS standards using either a baghouse or an ESP for particulate removal. The concentration of priority pollutant organics in ash/seed samples was about the same or less as from conventional coal-burning plants. No difficulty is expected in disposing of ash or slag from commercial MHD plants.

6.7. Plant Control, Part Load Performance, and Availability

Conventional power plant control practices, ie, conventional boiler-following, turbine-following, or coordinated control strategies, are all applicable, with some modifications, to the operation of MHD–steam power plants. These can provide for attractive load following characteristics, plant stability, and safe operation (142). Special control actions to safeguard plant equipment during emergencies and abnormal operating conditions such as sudden loss of MHD generator load are part of the overall plant control strategy.

The MHD generator itself has practically instantaneous response characteristics compared to the steam bottoming plant. Thus the load following capabilities and dynamic response of the overall plant are dominated by the bottoming steam plant and oxidant supply system. However, stringent requirements are imposed on reactant mass flow rates because these affect power generation. Also, outputs from external electrical circuits are affected by inputs from gasdynamic variables internal to the MHD channel. These inputs cannot in all cases be measured directly, and so must be inferred from external measurements by use of computer algorithms (143).

Assessments of control, operability and part load performance of MHD–steam plants are discussed elsewhere (r144 and r145). Analyses have shown that relatively high plant efficiency can be maintained at part load, by reduction of fuel input, mass flow, and MHD combustor pressure. In order to achieve efficient part load operation the steam temperature to the turbine must be maintained. This is accomplished by the use of flue gas recirculation in the heat recovery furnace at load conditions less than about 75% of full load.

Reliability, availability, and maintainability are critical factors in the use of MHD for electric utility power generation. The duration and lifetime requirements of the principal components and subsystems of an MHD–steam power plant have been assessed in relation to the requirements of acceptable overall plant reliability and availability (146). Duration and reliability of the MHD generator channel are critical factors. The concept of using a stand-by spare channel for scheduled replacement of the operating channel after a certain operating time is both practical and cost effective. Planned maintenance is expected to be a significant

factor in avoiding forced outages and in achieving high availability of the MHD generator channel as well as other plant equipment and the overall power plant.

7. Development Programs

The U.S. national MHD development program (147) was funded by the U.S. Department of Energy (DOE), through the Pittsburgh Energy Technology Center. The program objectives were to establish, through proof of concept (POC) testing, an engineering database so that the risks and benefits of the technology can be evaluated by the private sector before proceeding with commercial demonstration. The POC program was aimed at performance and lifetime of principal components and subsystems. The national program also included conceptual designs of possible MHD pilot-scale plants.

The principal test programs were conducted at two DOE test facilities, the integrated topping cycle at the 50 MW_t Component Development and Integration Facility (CDIF), in Butte, Montana (148), and the integrated bottoming cycle activities at the 28 MW_t Coal Fired Flow Facility (CFFF), in Tullahoma, Tennessee (149). The CDIF has a complete coal-fired MHD power train, a 3 T iron core magnet, and an inverter which interfaces with the local utility grid. The CFFF has a complete HRSR system fired by a coal-fired flow train, but does not operate with a magnet.

7.1. Conceptual Design of MHD Repowered Plant

The first step toward MHD plant commercialization is a pilot-scale demonstration plant. Repowering of existing plants, actively under study both in the United States and elsewhere (65), allows use of existing systems at considerable cost savings compared to building a new plant from the ground up. It also ensures that the pilot scale demonstration occurs in a realistic utility environment and with utility participation. Existing power plant systems which can be used include the steam turbine and generator, principal parts of the cooling water system, the electrical transmission system, waste handling, auxiliary support systems such as fire protection, heating, ventilation and plant utilities, and, of course, the site itself.

Conceptual designs of two repowered existing coal-fired plants in the United States, the Montana Power Company's Corlette plant in Billings, Montana, and Gulf Power's Scholz plant, in Sneads, Florida are described in References 150 and 151.

7.2. Integrated Topping Cycle

The objective of the integrated topping cycle program was to build and test, for a total of 1000 hours, an integrated coal-fired MHD flow train consisting of a combustor, nozzle, channel, associated power conditioning equipment, and diffuser. The flow train and the operating conditions are intended to be prototypical of hardware for commercial plants, so that design and operating data can be used to project component performance, lifetime, and reliability in commercial plants. The flow train operated at 50 MW_t. The program was conducted by a team led by TRW, Inc., and included Textron Defense Systems and Westinghouse Electric Corp. The integrated topping cycle operation followed an earlier program of component testing at the CDIF, and concluded in 1993, when program funding was terminated, with over 500 hours of accumulated operating time, of which over 300 hours were at design power-generating conditions (152, 153).

In order to support the design and fabrication of the prototypical flow train, extensive component testing at the 50 MW_t level was performed at the CDIF, in addition to testing of electrodes and sidewalls and of coal-fired channels of 20 MW_t size at Textron Defense Systems.

7.3. Integrated Bottoming Cycle

The bottoming cycle program was conducted with a heat recovery and seed recovery system, located at the CFFF in Tullahoma, Tennessee. The system includes a radiant furnace, secondary combustor, air heaters, superheater modules, cyclone scrubbers, a baghouse, and an electrostatic precipitator. It was fired by a coal-fired flow train rated at 28 MW_t. Long-term testing was conducted, with the goal of obtaining 2000 hours of operation on each of two types of coal: Montana Rosebud, considered to be a representative low sulfur Western coal; and Illinois No. 6, a representative high sulfur Eastern coal. The goal of the integrated bottoming cycle program was to obtain an engineering database for the heat recovery and seed recovery (HRSR) components of the bottoming cycle, so that operational characteristics, reliability, maintainability, and materials performance applicable to commercial systems can be established. The program was conducted by the University of Tennessee Space Institute, with assistance from Babcock and Wilcox Corp. A small program to provide supplemental materials test data was in place at Argonne National Laboratory.

The bottoming cycle components used existing boiler technology and materials wherever possible (see Combustion technology). Appropriate gas-side conditions were provided by a coal-fired flow train which simulated as closely as possible the composition, temperature, and residence time, among other conditions, in a commercial MHD-steam plant. Specific aspects of system operation investigated included slagging, fouling, erosion, and corrosion of heat transfer surfaces; identification, control, and measurements of gaseous and particulate pollutants; waste management; seed recovery; heat transfer; and system integration and scaling characteristics.

7.4. Seed Regeneration

The objectives of the seed regeneration program were to provide experimental verification of the feasibility of one of the seed regeneration processes which have been selected for first commercial use. The specific process under evaluation was the Econoseed process (Fig. 11) (61). A 5 MW_t POC facility was in operation in Capistrano, California, and produced over 6 t of potassium formate seed, which was regenerated from spent seed, ie, K₂SO₄, obtained from CFFF tests.

7.5. International MHD Programs

A number of countries are conducting programs in coal-fired MHD power generation. Detailed descriptions of these programs can be found in Reference 65. A summary is given in Table 6.

Coal-fired power generation for hundreds of hours, at conditions representative of those projected for commercial plants, has been demonstrated at 50 MW_t scale at the CDIF test site in Butte, Montana. Satisfactory operation of the primary flow train components, the slag-rejecting coal combustor, and the channel has been demonstrated, as has operation of the primary ancillary systems: the coal feed system and the slag rejection system of the coal combustor, and the power conditioning, inversion, and transmission systems of the channel. Elsewhere, channel enthalpy extraction meeting pilot-scale requirements has been demonstrated, and large superconducting MHD magnets have been built and tested.

Thousands of hours of bottoming cycle operations at the CFFF (Tullahoma, Tennessee), have generated a substantial engineering database for the design of future commercial MHD bottoming plants. Operations with both high and low sulfur coals have verified projections that SO_x and NO_x emissions are well below current and expected future standards. A pilot-scale seed regeneration plant has been built and has demonstrated the technical viability of the formate seed regeneration process.

Table 6. National MHD Programs,^d

Country	Organization	Location	Facility ^a	Thermal input, MW	Magnetic field, T ^b	Test duration, h	Comments
Australia	University of Sydney, School of Electrical Engineering	White Bay Power Station	disk gen-erator	2	2.7	36 ^c	basic generator research studies of coal-fired MHD in progress
China	Shanghai Power Equipment Research Institute	Shanghai		25	4.5	1000 ^e	MHD–steam combined cycle generator proposed
		Shanghai	SMS	5		60	coal-fired bottoming cycle test facility
	Institute of Electrical Engineering	Beijing		25	1.9		coal-fired flow train in operation 4 T superconducting magnet under construction
India	Bharat Heavy Electricals	Tiruchirapalli	pilot plant	5	2	up to 150 ^f	5 MW pilot plant in operation; 3 MW coal combustor test facility also in operation
Italy	Industrial MHD Consortium/Ansaldo CNR/Ansaldo	Geneva	MDA	1	1.4		gas-fired test facility
		Geneva					5 T, 62 M MHD superconducting magnet under construction
Japan	Industrial MHD Consortium	University of Bologna					design of 230 MW _t MHD pilot plant in progress
	Tokyo Institute of Tech	Yokohama	FUJI-1	2–3			closed cycle disk facility; 30% enthalpy extraction achieved
	Hokkaido University Kyoto University	Hokkaido	MDX-1	5	2.5		oil-fired open cycle test facility
	Toyohashi University of Technology	Toyohashi			2		analytical studies, computer simulations
Romania	ICPET	Bucharest	G MHD-03	1–2.5			experimental studies of electrode phenomena
Russia	Institute of High Temp	Moscow	U-25G	25	3.5		coal-fired MHD combustor studies
		Moscow	U-02	5	1.5–2	100s	integrated facility originally gas-fired, now coal-fired
	Krzhizhanovski Power Institute	Moscow	M-25	25			material test facility
	Institute of Energy Saving Problems, Ukrainian SSR Academy of Sciences	Kiev	K-1	15	1.8		channel development; electrophysical investigations of electrical discharge and interelectrode breakdown

^aSee text.^bTo convert T to G, multiply by 10⁴^cCumulative.^dClean fuel was used.^eContinuous generation.^fLPG was used as fuel.

7.5.1. Nomenclature

Symbol	Definition
A	flow area
B	flux density, magnetic field, magnetic induction
c	random thermal speed of particle
e	electron charge
\vec{E}	electric field in laboratory coordinates
\vec{E}'	sum of electrical and motional emf ($\vec{E}' = \vec{E} + \vec{u} \times \vec{B}$)
\vec{E}''	electric field felt by particles with drift velocity relative to the fluid
E_x	Hall field
F	body force
$f(v)$	velocity distribution function
g	statistical weight
h	specific flow enthalpy, Planck's constant
j	current density
k	Boltzmann constant, 1.38×10^{-23} J/K
K	generator load coefficient
K'	Hall generator load coefficient
m	mass
\dot{m}	mass flow rate
n	number density
p	pressure
P	power density
Q	collision cross-section
T	temperature
u	flow speed
\vec{u}	velocity
\bar{v}	mean drift velocity
MW_t	thermal megawatt
MW_e	electric megawatt
Z_k	number of charges on particle of species k
α	mole ratio at equilibrium
β	Hall parameter
ϵ	ionization potential
ϵ_o	permittivity of free space
η_e	efficiency
θ	diagonal connection angle
μ	mobility
ν	collision frequency
ρ	density
σ	electrical conductivity
<i>Subscripts</i>	
e	electron
i	ion
k	species identification
x	axial direction
y	transverse direction
z	direction parallel to magnetic field

BIBLIOGRAPHY

“Power from Coal by Gasification and Magnetohydrodynamics” in *ECT* 2nd ed., Suppl. Vol., pp. 217–249, by S. Way, Westinghouse Electric Corp.; “Coal Conversion Processes (MHD)” in *ECT* 3rd ed., Vol. 6, pp. 324–377, by S. Way, Consultant.

Cited Publications

1. M. Faraday, *Philos. Trans. R. Soc.*, 125–162 (1832).
2. B. Karlovitz and D. Halasz, in N. W. Mather and G. W. Sutton, eds., *Proc. of 3rd Symposium on Engineering Aspects of MHD*, Gordon and Breach Science Publishers, Inc., New York, 1964, 187–204.
3. R. J. Rosa, *J. Appl. Phys.* **31**, 735–736 (Apr. 1960); also *Avco Everett Res. Lab. Rept. AMP 42* (Jan. 1960).
4. R. J. Rosa, *Phys. Fluids* **4**, 182–194 (Feb. 1961); also *Avco Everett Res. Lab. Rept. RR 69* (Jan. 1960).
5. S. C. Lin, E. L. Resler, and A. R. Kantrowitz, *J. Appl. Phys.* **26**(1), 83–95 (Jan. 1955); H. E. Petschek, *Approach to Equilibrium behind Strong Shock Waves in Argon*, Ph.D. dissertation, Cornell University, Ithaca, N.Y., 1955; R. M. Patrick, *Magnetohydrodynamics of a Compressible Fluid*, Ph.D. dissertation, Cornell University, Ithaca, N.Y., 1956; R. J. Rosa, *Engineering Magnetohydrodynamics*, Ph.D. dissertation, Cornell University, Ithaca, N.Y., 1956; J. Jukes, *Ionic Heat Transfer to the Walls of a Shock Tube*, Ph.D. dissertation, Cornell University, Ithaca, N.Y., (1956).
6. S. Way and co-workers, *J. Eng. Power*, **83A**, 397 (1961).
7. J. F. Louis, J. Lothrop, and T. R. Brogan, *Phys. Fluids* **7**(3), 362–374 (Mar. 1964); also *Avco Everett Res. Lab. Rept. RR 145* (Mar. 1963).
8. R. B. Boulay and co-workers, in *Proc. of 10th International Conference on MHD Electrical Power Generation*, Tiruchirapalli, India, Dec. 1989, pp. IX.139–IX.145.
9. B. Zaporowski and co-workers, in *Proc. of 11th International Conference on MHD Electrical Power Generation*, Beijing, Oct. 1992, 106–113.
10. V. K. Rohatgi and co-workers, in *Proc. of 6th International Conference on MHD Electrical Power Generation*, Washington, D.C., June 1975, 45–59.
11. M. Petrick and B. Ya. Shumyatsky, eds., *Open Cycle MHD Electrical Power Generation*, Argonne National Laboratory, Argonne, Ill., 1978, 16–48.
12. S. Hamilton, in *Proc. of 2nd Symposium on Engineering Aspects of MHD*, Columbia University Press, New York, 1962, 211–227.
13. K. Yoshikawa and co-workers, in *Proc. of 31st Symposium on Engineering Aspects of MHD*, Whitefish, Mont., June 1993, pp. IVb 3.1–IVb 3.7.
14. J. Carrasse, in *Electricity from MHD, Proceedings of the Salzburg Symposium*, Vol. **3**, Salzburg, July 1966, p. 883.
15. F. Hals and R. Gannon, *Proc. of 13th Symposium on Engineering Aspects of MHD*, Stanford, Calif., Mar. 1973, pp. V.3.1–V.3.10.
16. R. E. Gannon and co-workers, in *Proc. of 14th Symposium on Engineering Aspects of MHD*, Tullahoma, Tenn., Apr. 1974, pp. II.2.1–II.2.8.
17. W. S. Brzozowski and co-workers, in Ref. 10, 137–154.
18. V. I. Kovbasiuk and co-workers, in *Proc. of 30th Symposium on Engineering Aspects of MHD*, Baltimore, Md., June 1992, pp. IV.3.1–IV.3.5.
19. O. V. Bystrova and co-workers, in Ref. 9, 114–121.
20. T. G. Cowling, *Magnetohydrodynamics*, Interscience Publishers Inc., New York, 1957, Chapt. 6.
21. J. Louis, “Studies on an Inert Gas Disk Hall Generator Driven in A Shock Tunnel,” *Proc. of 8th Symposium on Engineering Aspects of MHD*, Stanford, Calif., Mar. 1967.
22. C. du P. Donaldson, in Ref. 12, 228–254.
23. A. de Montardy, *Proc. of First International Symposium on MHD Electric Power Generation*, Newcastle on Tyne, U.K., 1962.
24. N. Harada and co-workers, in Ref. 18, pp. IX.5.1–IX.5.9.
25. N. Harada and co-workers, in Ref. 13, pp. IV.2.1–IV.2.9.
26. V. G. Kirillov and co-workers, in Ref. 9, 658–665.
27. S. W. Simpson and co-workers, in Ref. 18, pp. IV.6.1–IV.6.5.

28. J. Gertz and co-workers, in *Proc. of 18th Symposium on Engineering Aspects of MHD*, Butte, Mont., June 1979, pp. B.4.1–B.4.9.
29. C. C. P. Pian and A. W. McClaine, *Computers and Fluids* **12**(4), 319–338 (1984).
30. S. T. Demetriades and co-workers, in *Proc. of 12th Symposium on Engineering Aspects of MHD*, Argonne, Ill., Mar. 1972, pp. I.5.1–I.5.13.
31. S. Gordon and B. McBride, *Computer Program for Calculation of Complex Chemical Equilibrium Compositions*, NASA SP-273, National Aeronautics and Space Administration, Washington, D.C., 1971.
32. J. C. Cutting and co-workers, in *Proc. of 16th Symposium on Engineering Aspects of MHD*, Pittsburgh, Pa., May 1977, pp. VII.4.21–VII.4.26.
33. C. D. Maxwell and co-workers, in Ref. 32, pp. VII.3.13–VII.3.20.
34. G. W. Sutton and A. Sherman, *Engineering Magnetohydrodynamics*, McGraw-Hill Book Co., Inc., New York, 1965, Chapt. 5.
35. R. J. Rosa, *Magnetohydrodynamic Energy Conversion*, McGraw-Hill Book Co., Inc., New York, 1968, Chapt. 2.
36. M. W. Zemansky, *Heat and Thermodynamics*, 3rd ed., McGraw-Hill Book Co., Inc., New York, 1951, 412–414.
37. L. S. Frost, *J. Appl. Phys.* **32**(10), 2029–2036 (Oct. 1961).
38. W. P. Allis, *Handbuch der Physik*, Vol. **21**, Springer-Verlag, Berlin, 1956, pp. 413.
39. L. Spitzer and R. Harm, *Phys. Rev.* **89**, 977 (1953).
40. L. Spitzer, Jr., *Physics of Fully Ionized Gases*, 2nd ed., Interscience Publishers, Inc., New York, 1962, Chapt. 5.
41. G. Seikel and co-workers, in *Proc. of 15th Symposium on Engineering Aspects of MHD*, Philadelphia, Pa., May 1976, pp. III.4.1–III.4.22.
42. *Evaluation of Phase 2 Conceptual Designs and Implementation Assessment Resulting from the Energy Conversion Alternatives Study (ECAS)*, NASA TM X-73515, NASA Lewis Research Center, Cleveland, Ohio, Apr. 1977.
43. B. D. Pomeroy and co-workers, *Comparative Study and Evaluation of Advanced Cycle Systems*, Electric Power Research Institute, Palo Alto, Calif., Report AF-664, 1, Feb. 1978.
44. F. Hals and co-workers, in *Proc. of 20th Symposium on Engineering Aspects of MHD*, Irving, Calif., June 1982, pp. 1.1.1–1.1.9.
45. General Electric Co., *Definition of the Development Program for an MHD Advanced Power Train*, DOE Report No. DE-AC22-83PC60574, U.S. Department of Energy, Washington, D.C., Dec. 1984.
46. R. E. Weinstein and R. B. Boulay, in *Proc. of 26th Symposium on Engineering Aspects of MHD*, Nashville, Tenn., June 1988, pp. 8.5.1–8.5.9.
47. J. Zeldovich, *Acta. Physicochim.* **21**, 577 (1946).
48. F. A. Hals and P. F. Lewis, in Ref. 30, pp. VI.5.1–VI.5.10.
49. J. Klinger and co-workers, in *Proc. of 22nd Symposium on Engineering Aspects of MHD*, Starkville, Miss., June 1984, pp. 10.2.1–10.2.20.
50. J. W. Pepper and C. H. Kruger, in Ref. 15, pp. VII.2.1–VII.2.3.
51. J. W. Pepper, *Effect of Nitric Oxide Control on MHD-Steam Power Plant Economics and Performance*, SU-IPR Report No. 614, Institute for Plasma Research, Stanford University, Calif., Dec. 1974.
52. L. W. Crawford and co-workers, “Nitrogen-Oxide Control in a Coal-Fired MHD System,” *Proc. of 21st Symposium on Engineering Aspects of MHD*, suppl. vol., Argonne, Ill., June 1983.
53. A. C. Sheth and co-workers, “MHD Can Clean Up The Environment,” *Proceedings of the American Power Conference*, Chicago, Apr. 1993.
54. J. Lanier and co-workers, “Sulfur Dioxide and Nitrogen Oxide Emissions Control in a Coal-Fired MHD System,” *ASME Winter Annual Meeting*, Atlanta, Ga., Dec. 1979.
55. D. G. Rasnake and co-workers, in *Proc. of 29th Symposium on Engineering Aspects of MHD*, New Orleans, La., June 1991, pp. V.1.1–V.1.8.
56. E. J. Lahoda and T. E. Lippert, in Ref. 28, pp. C.3.1–C.3.6.
57. P. Bergman and co-workers, in Ref. 32, pp. X.3.11–X.3.23.
58. J. K. Holt and co-workers, in Ref. 8, pp. XI.80–XI.85.
59. A. C. Sheth and co-workers, in Ref. 8, pp. IX.86–IX.93.
60. A. C. Sheth and co-workers, in Ref. 13, pp. IX.9.1–IX.9.12.
61. R. A. Meyers and co-workers, in Ref. 46, pp. 12.3.1–12.3.10.
62. J. L. Anastasi and co-workers, in Ref. 18, pp. II.4.1–II.4.12.

63. R. C. Attig and co-workers, in *Proc. of 27th Symposium on Engineering Aspects of MHD*, Reno, Nev., June 1989, pp. 1.2-1-1.2-9.
64. Ref. 8, pp. III.1-III.78.
65. Ref. 9, 3-74.
66. J. N. Chapman and N. R. Johanson, "Design Considerations for a Class of 600 MWe MHD Steam Combined Cycle Plants," *28th Intersociety Energy Conversion Engineering Conference*, Atlanta, Ga., Aug. 1993.
67. J. B. Heywood and G. J. Womack, eds., *Open Cycle MHD Power Generation*, Pergamon Press, London, 1969, 18-158.
68. D. P. Saari, in Ref. 21, pp. I.8.1-I.8.8.
69. Yu. A. Gorshkov and co-workers, in Ref. 9, 1033-1039.
70. S. Way, *Combustion Technology, Some Modern Developments*, Academic Press, Inc., New York, 1974.
71. H. Seidl, *Proceedings Joint Symposium on Combustion*, Institute of Mechanical Engineers, London, (1955); H. Seidl, *Eleventh Coal Science Lecture*, Inst. of Civil Engineers, Publ. Gazette, 46, British Coal Utilization Research Assoc., Leatherhead, U.K., Oct. 1962.
72. D. Q. Hoover and co-workers, *Feasibility Study of Coal Burning MHD Generation*, Contract 14-01-001-476, Westinghouse Research Laboratories, Pittsburgh, Pa., (1966); S. Way and co-workers, internal company report, Westinghouse Research Labs, Pittsburgh, Pa., Nov. 5, 1963; U.S. Pat. 3,358,624 (Dec. 19, 1967), S. Way (to Westinghouse).
73. M. Bauer and co-workers, in Ref. 44, pp. 3.3.1-3.3.8.
74. G. Listvinsky and co-workers, in Ref. 8, pp. IX.42-IX.47.
75. G. Roy and A. Solbes, in Ref. 49, pp. 6:4.1-6:4.21; A. Solbes and G. Listvinsky, in Ref. 13, pp. XII.2.1-XII.2.17.
76. C. A. Hauenstein and co-workers, in *Proc. of 19th Symposium on Engineering Aspects of MHD*, Tullahoma, Tenn., June 1981, pp. 16.2.1-16.2.4.
77. J. O. A. Stankevics and co-workers, in Ref. 44, pp. 3.1.1-3.1.11.
78. Sha Ciwen and co-workers, in *Proc. of 23rd Symposium on Engineering Aspects of MHD*, Somerset, Pa., June 1985, 109-113.
79. S. A. Arunachalam and co-workers, in Ref. 63, pp. 7.4-1-7.4-4.
80. W. Zheng and co-workers, in Ref. 8, pp. IX.7-IX.11.
81. M. Akai and co-workers, in Ref. 8, pp. IX.16-IX.23.
82. J. B. Dicks and co-workers, in Ref. 16, pp. II.1-II.1.10.
83. B. L. Liu and H. J. Schmidt, in Ref. 78, 479-490.
84. T. V. Velikaya and G. E. Goryainov, in Ref. 8, pp. IX.52-IX.57.
85. J. E. Cox, in Ref. 49, pp. 6.2.1-6.2.16.
86. L. C. Farrar and co-workers, in Ref. 78, 879-887.
87. R. T. Burkhart, in Ref. 18, pp. V.3.1-V.3.3.
88. G. Roy, in *Proc. of 24th Symposium on Engineering Aspects of MHD*, Butte, Mont., June 1986, 131-136.
89. A. E. Sheindlin and co-workers, in *4th US-USSR Colloquium on MHD Electrical Power Generation*, Washington, D.C., Oct. 1978, 87-104.
90. R. Kessler, *J. Energy*, 178-184, (1981).
91. S. W. Petty and co-workers, in Ref. 32, pp. VIII.1.1-VIII.1.12.
92. V. J. Hruby and P. Weiss, in Ref. 76, pp. 2.2.1-2.2.20.
93. I. Sadovnik and co-workers, in Ref. 44, pp. 4.2.1-4.2.9.
94. A. Solbes and A. Lowenstein, in Ref. 41, pp. IX.3.1-IX.3.7.
95. A. Demirjian and co-workers, in *Proc. of 17th Symposium on Engineering Aspects of MHD*, Stanford, Calif., Mar. 1977, pp. D1.1-D1.6.
96. J. K. Koester and R. M. Nelson, in Ref. 32, pp. VI.2.5-VI.2.12.
97. E. K. Keler, in *3rd US-USSR Colloquium on MHD Electrical Power Generation*, Moscow, Oct. 1976, 405-412.
98. G. P. Telegin and co-workers, in Ref. 97, 413-431.
99. Ya. P. Gokhstein and co-workers, in Ref. 89, 637-685.
100. A. M. George and co-workers, in Ref. 41, pp. II.1.1-II.1.5.
101. Session XI, in Ref. 9, 853-950.
102. V. J. Hruby and co-workers, in Ref. 44, pp. 4.3.1-4.3.6.
103. A. M. Demirjian and co-workers, in Ref. 28, pp. A.3.1-A.3.11.
104. S. W. Petty and co-workers, *Proceedings of the 29th Symposium on Engineering Aspects of MHD*, New Orleans, La.,

- June 1991, pp. 11.1.1–11.1.10.
105. S. Petty and co-workers, in Ref. 41, pp. IV.5.1–IV.5.10.
 106. R. F. Starr and co-workers, in *Proc. of 7th International Conference on MHD Electrical Power Generation*, Vol. 3, Cambridge, Mass., June 1980, 203–217.
 107. J. Teno and co-workers, *Proc. of 10th Symposium on Engineering Aspects of MHD*, Cambridge, Mass., Mar. 1969, 194–200.
 108. K. D. Kuczen and co-workers, in Ref. 106, Vol. 1, 195–201.
 109. A. E. Barshak in Ref. 95, pp. F.2.1–F.2.9.
 110. V. A. Kirillin and co-workers, in Ref. 95, pp. F.1.1–F.1.12.
 111. L. Whitehead and co-workers, paper presented at *MHD Contractors' Review Meeting*, Pittsburgh, Pa., Nov. 1983.
 112. J. Sherick and co-workers, in Ref. 9, 62–65; W. R. Owens and co-workers, in Ref. 9, 65–74.
 113. B. M. Antonov and co-workers, in Ref. 89, 543–570.
 114. A. Lowenstein in Ref. 76, pp. 17.1.1–17.1.6.
 115. A. Lowenstein, in Ref. 95, pp. I.1.1–I.1.6.
 116. R. J. Rosa, in Ref. 41, pp. VII.5.1–VII.5.4.
 117. R. Putkovich, in Ref. 63, pp. 8.11.1–8.11.9.
 118. Y. Inui and co-workers, in Ref. 8, pp. XIII.2–XIII.9.
 119. V. J. Hruby and co-workers, in Ref. 78, 804–824.
 120. I. Sadovnik and V. J. Hruby, in Ref. 78, 790–803.
 121. J. Reich and co-workers, in Ref. 55, pp. IX.3.1–IX.3.8.
 122. Ref. 11, 275–318.
 123. E. Ray and R. Schainker, in Ref. 106, Vol. 1, 421–425.
 124. B. M. Antonov and co-workers, in Ref. 106, Vol. 1, 410–420.
 125. A. Chaffee and co-workers, in Ref. 28, pp. F.1.1–F.1.10.
 126. P. G. Marston and co-workers, in *Proc. 11th International Conference on Magnet Technology*, Vol. 2, MT-11, Elsevier Applied Science, London, 1989, 920–925.
 127. P. G. Marston and co-workers, *IEEE Trans. Mag.* **28**, 271–274 (1992).
 128. R. W. Baldi, in Ref. 106, 433–439.
 129. F. Negrini and co-workers, in Ref. 18, pp. I.1.1–I.1.10.
 130. T. Okamura and co-workers, in *International Workshop on MHD Superconducting Magnets*, Nov. 1991, 13–15.
 131. Y. Aiyama and co-workers, in *Proceedings of the Fourth International Cryogenics Engineering Conference*, Eindhoven, 1972, 227–229.
 132. V. A. Kirillin and co-workers, in Ref. 95, pp. F.1.1–F.1.12.
 133. S.-T. Wang and co-workers, *Cryogenics* **22**, 335 (1982); Argonne National Laboratory, in Ref. 53, suppl. vol.
 134. R. Rajaram, in Ref. 18, pp. 7.1–7.12.
 135. Ref. 11, 465–487.
 136. K. V. S. Sundaram, in Ref. 55, pp. V.2.1–V.2.6.
 137. F. Hals, "Conceptual Design Study of Potential Early Commercial MHD Power Plant," *NASA CR-165235*, NASA Lewis Research Center, Cleveland, Ohio, Mar. 1981, 3–60.
 138. G. F. Berry in Ref. 88, 167–174.
 139. M. K. White and M. Li, in *Proc. of 28th Symposium on Engineering Aspects of MHD*, Chicago, 1990, pp. VII.5.1–VII.5.12.
 140. K. Natesan and W. M. Swift, in Ref. 63, pp. 3.2.1–3.2.10.
 141. M. K. White, in Ref. 63, pp. 3.1.1–3.1.8.
 142. D. A. Rudberg and co-workers, in Ref. 76, pp. 14.3.1–14.3.9.
 143. D. Lofftus and co-workers, in Ref. 13, pp. X.6.1–X.6.14.
 144. M. Ishikawa and co-workers, in Ref. 8, pp. III.36–III.43.
 145. M. L. R. Murthy and co-workers, in Ref. 76, pp. 6.2.1–6.2.5.
 146. F. D. Retallick and co-workers, in Ref. 28, pp. H.2.1–H.2.5.
 147. R. J. Wright, in Ref. 9, 1365–1371.
 148. A. T. Hart and co-workers, in Ref. 63.
 149. N. R. Johanson and J. W. Muehlhauser, "MHD Bottoming Cycle Operations and Test Results at the CFFF," paper presented at *Second International Workshop on Fossil Fuel Fired MHD*, Bologna, Italy, 1989.

54 MAGNETOHYDRODYNAMICS

- 150. R. Labrie and co-workers, in Ref. 8, pp. II.63–II.69.
- 151. L. Van Bibber and co-workers, in Ref. 8, pp. II.58–II.62.
- 152. C. C. P. Pian and co-workers, in Ref. 13, pp. II.2.1–II.2.11.
- 153. C. C. P. Pian and E. W. Schmitt, in *Proceedings of the 32nd Symposium on Engineering Aspects of MHD*, Pittsburgh, Pa., June 1994, Session 2.

General References

- 154. R. J. Rosa, *Magnetohydrodynamic Energy Conversion*, McGraw-Hill Book Co., Inc., New York, 1968.
- 155. G. W. Sutton and A. Sherman, *Engineering Magnetohydrodynamics*, McGraw-Hill Book Co., Inc., New York, 1965.
- 156. M. Petrick and B. Ya. Shumyatsky, eds., *Open Cycle MHD Electrical Power Generation*, Argonne National Laboratory, Argonne, Ill., 1978.
- 157. J. B. Heywood and G. J. Womack, eds., *Open Cycle MHD Power Generation*, Pergamon Press, London, 1969.
- 158. Published proceedings of: *Symposium on Engineering Aspects of Magnetohydrodynamics*, annually since 1961; *International Conference on Magnetohydrodynamic Electrical Power Generation*, every 3–4 years since 1962.

ROBERT KESSLER
Textron Defense Systems

Related Articles

Air pollution control methods; Wastes, industrial; Coal conversion processes; Fuels, synthetic; Magnetic materials; Heat-exchange technology